

## **An improved general fast radiative transfer model for the assimilation of radiance observations.**

Marco Matricardi, Frederic Chevallier,  
Stephen Tjemkes<sup>1</sup>

Research Department

<sup>1</sup> EUMETSAT, , Darmstadt, Germany.

May 2001

**For additional copies please contact**

The Library  
ECMWF  
Shinfield Park  
Reading, Berks RG2 9AX

library@ecmwf.int

**Series: ECMWF Technical Memoranda**

A full list of ECMWF Publications can be found on our web site under:  
<http://www.ecmwf.int/pressroom/publications.html>

**© Copyright 2001**

European Centre for Medium Range Weather Forecasts  
Shinfield Park, Reading, Berkshire RG2 9AX, England

Literary and scientific copyrights belong to ECMWF and are reserved in all countries. This publication is not to be reprinted or translated in whole or in part without the written permission of the Director. Appropriate non-commercial use will normally be granted under the condition that reference is made to ECMWF.

The information within this publication is given in good faith and considered to be true, but ECMWF accepts no liability for error, omission and for loss or damage arising from its use.



## Summary

An improved version of the RTTOV fast radiative transfer model used operationally at the European Centre for Medium-Range Weather Forecasts for the assimilation of advanced TIROS operational vertical sounder radiances has been developed. This new model compute radiances for the Atmospheric Infrared Sounder and reproduce line-by-line radiances and Jacobians for the surface sensing, water vapour and ozone channels of the advanced TIROS operational vertical sounder with significantly improved accuracy. The profile-dependent predictors used by the improved model to parameterise the atmospheric optical depths are based on the approach followed by RTIASI, the ECMWF fast radiative transfer model for the Infrared Atmospheric Sounding Interferometer. To improve the accuracy of the fast model in reproducing line-by-line radiances for the Atmospheric Infrared Sounder, modifications have been made to the predictors used in RTIASI by introducing a revised set of predictors for ozone and adding new predictors to model the water vapour continuum type absorption. To eliminate discontinuities in the water vapour Jacobians observed in RTIASI, data are now weighted prior to performing the regression.

Keywords: Data assimilation Numerical weather prediction Radiative Transfer

## 1. INTRODUCTION

Radiances from the Advanced TIROS Operational Vertical Sounder (ATOVS) on the National Oceanic and Atmospheric Administration (NOAA) polar orbiting satellites are used at the European Centre for Medium-Range Weather Forecasts (ECMWF) by assimilating the radiances directly into the four-dimensional variational analysis scheme (Rabier et al. 1998). One step forward in the objective of making improvements in NWP models will be the availability of high-resolution infrared sounder data on operational polar orbiters which will provide temperature and constituents profiles at a higher accuracy and with more vertical resolution than the existing filter wheel radiometers. The Atmospheric Infrared Sounder (AIRS) has been designed for the next generation of operational meteorological polar orbiters. AIRS (Aumann and Pagano, 1994) is an instrument selected by the National Aeronautic and Space Administration (NASA) to fly on the second Earth Observing System (EOS) polar orbiting platform, EOS-PM 1. In combination with the Advanced Microwave Sounding Unit (AMSU) it will provide improved information on meteorological parameters for NWP and climate models.

Given the potential benefits of AIRS for NWP, preparations are being made at ECMWF for exploitation of the AIRS datasets. A prerequisite for exploiting radiance data from conventional and high-resolution satellite sounders is the availability of a fast radiative transfer model (usually called the observation operator) to predict a first guess radiance from the model fields (temperature, water vapour, ozone, surface emissivity and perhaps clouds at a later time) corresponding to every measured radiance. The minimisation procedure involved in 4D-Var requires the computation of the gradient of the cost function (measuring a weighted departure between the observation and the model equivalent) with respect to the atmospheric profile. The radiative transfer model and its adjoint are therefore a key component to enable the assimilation of satellite radiance in a NWP system.

The parameterisation of the transmittances used in RTTOV-5, the fast radiative transfer model currently operational at ECMWF (Saunders et al. 1999), makes the model computationally efficient and in principle should not add significantly to the errors generated by uncertainties in the spectroscopic data used by the line-by-line (LBL) model on which the fast model is based. While for the ATOVS stratospheric temperature sounding channels the model can reproduce LBL model radiances to an accuracy below the instrumental



noise, for the surface sensing, ozone and, most importantly, water vapour channels, errors introduced by the parameterisation of the transmittances are above the instrumental noise and can be a significant fraction of the errors introduced by spectroscopic uncertainties in the LBL model (Rizzi et al. 2001). It has also been shown (Garand et al. 2001) that significant differences exist between Jacobians computed using RTTOV-5 and a LBL model. Since the Jacobian is a fundamental quantity in the direct assimilation of satellite radiance in an NWP model (analysis increments will differ if Jacobians differ) it is desirable to improve the accuracy of the operational fast model Jacobians.

A fast radiative transfer, RTAIRS (Radiative Transfer for AIRS) model has been developed at ECMWF for exploitation of AIRS radiances that is based on the approach followed by RTIASI (Matricardi and Saunders, 1999). It contains a fast model of the transmittances of the atmospheric gases that is generated from accurate LBL transmittances for a set of diverse atmospheric profiles over the AIRS wave-number range. The monochromatic transmittances are convolved with the appropriate instrument spectral response function and are used to compute channels-specific regression coefficients by use of a selected set of predictors. These regression coefficients can then be used by the fast transmittance model to compute transmittances given any other input profile. As part of the effort to develop RTAIRS, modifications were made to the predictors used in RTIASI. A revised set of predictors was introduced for ozone and new predictors were added to model the water vapour continuum type absorption. A further modification to the methods used in RTIASI was the weighting of the data prior to performing the regression. This was effective in eliminating discontinuities in the water vapour Jacobians observed in RTIASI due to the split regime used there to model the water vapour transmittance.

The set of predictors developed for RTAIRS was implemented into the RTTOV-5 scheme to improve prediction of the High-Resolution Infra-Red Sounder (HIRS) channels. Results obtained by use of the new predictors demonstrate that a single set of predictors can be used to accurately reproduce LBL radiances for a wide range of satellite instruments, from the conventional infrared and microwave to the advanced high resolution sounders. As a result of this, a new version of RTTOV, RTTOV-7, has been jointly developed with Météo France and The Met Office that among the other new features includes the use of the new predictors and the possibility of supporting the AIRS instrument.

The methods that were applied to develop RTAIRS are described in section 2. In section 3 the performance of the fast model is described by comparing fast model transmittances and radiances with LBL equivalents. The performance of the improved RTTOV with new predictors is discussed in section 4. Conclusions are given in section 5.

## **2. THE FAST RADIATIVE TRANSFER MODEL FOR AIRS**

### **2.1 General description of the model**

RTAIRS is based on the methods developed for RTIASI. For a detailed description of RTIASI the reader can refer to Matricardi and Saunders (1999). Only the main components will be discussed here.

RTAIRS uses profile-dependent predictors to parameterise the atmospheric optical depths. Accurate LBL transmittances are computed for a set of diverse atmospheric profiles from 600 to 3000  $\text{cm}^{-1}$  and then convolved with the appropriate spectral response function. The convolved transmittances are used to



compute channel-specific regression coefficients by use of a selected set of predictors. Given these regression coefficients, the fast transmittance model can compute transmittances for any other input profile. Although the most recent data were used, uncertainties still remain regarding the shape of the spectral response function and the position of the channel centres of the AIRS instrument. It is anticipated that new regression coefficients will need to be generated after the instrument has stabilized in the space environment.

The atmosphere is divided into 43 layers defined by pressure levels from 0.005 hPa to 1013.25 hPa and is assumed to be plane-parallel in local thermodynamic equilibrium with no scattering. The model uses an approximate form of the radiative transfer equation based on the assumption that the same equation written for monochromatic radiances still apply when integrated over the spectral response of a satellite sounder channel. If  $\tilde{\nu}^*$  is the central wave-number of the AIRS channel, the clear column radiance at the top of the atmosphere can be written, in discrete layer notation for  $N$  atmospheric layers and for a single viewing angle to simplify the notation, as

$$\hat{L}_{\tilde{\nu}^*} = \hat{\tau}_{s,\tilde{\nu}^*} \varepsilon_{s,\tilde{\nu}^*} B_{\tilde{\nu}^*}(T_s) + \left( \sum_{j=1}^N \hat{L}_{j,\tilde{\nu}^*}^u \right) + (1 - \varepsilon_{s,\tilde{\nu}^*}) \left[ \sum_{j=1}^N \hat{L}_{j,\tilde{\nu}^*}^u \left( \frac{\tau_{s,\tilde{\nu}^*}^2}{\hat{\tau}_{j,\tilde{\nu}^*} \hat{\tau}_{j-1,\tilde{\nu}^*}} \right) \right] \quad (1)$$

where  $\hat{\tau}_{j,\tilde{\nu}^*}$  is the convolved transmittance from a given pressure level  $p_j$  to space,  $B_{\tilde{\nu}^*}(T)$  is the Planck's function for temperature  $T$  and  $\varepsilon_{s,\tilde{\nu}^*}$  is the surface emissivity; here the subscript  $s$  refers to the surface and  $\hat{\cdot}$  denotes convolution. In Eq. 1  $\hat{L}_{j,\tilde{\nu}^*}^u$  is defined as

$$\hat{L}_{j,\tilde{\nu}^*}^u = \frac{1}{2} [B_{\tilde{\nu}^*}(T_j) + B_{\tilde{\nu}^*}(T_{j-1})] (\hat{\tau}_{j,\tilde{\nu}^*} - \hat{\tau}_{j-1,\tilde{\nu}^*}) \quad (2)$$

The fast transmittance stage of RTAIRS is based on algorithms that have been developed over the years for a number of different satellite instruments (McMillin et al. 1979, Susskind et al. 1983, Eyre and Wolf 1988, Hannon et al. 1996). For a given input atmospheric profile (temperature, water vapour, and ozone volume mixing ratio) and surface variables (emissivity, pressure, temperature, skin temperature), the computation of the convolved level-to-space transmittance  $\hat{\tau}_{j,\tilde{\nu}^*}$  or convolved level-to-space optical depth  $\hat{\sigma}_{j,\tilde{\nu}^*}$  ( $\hat{\tau}_{j,\tilde{\nu}^*} = \exp[-\hat{\sigma}_{j,\tilde{\nu}^*}]$ ) is performed by the fast transmittance model and is the essence of RTAIRS. The computation of the optical depth for the layer from pressure level  $j$  to space along a path at angle  $2$  involves a polynomial with terms that are functions of temperature, absorber amount, pressure and viewing angle. The convolved optical depth at wave number  $\tilde{\nu}^*$  from level  $j$  to space can be written as:

$$\hat{\sigma}_{j,\tilde{\nu}^*} = \hat{\sigma}_{j-1,\tilde{\nu}^*} + \sum_{k=1}^M a_{j,\tilde{\nu}^*,k} X_{k,j} \quad (3)$$

where  $M$  is the number of predictors and the functions  $X_{k,j}$  constitute the profile-dependent predictors of the fast transmittance model. To compute the expansion coefficients  $a_{j,\bar{\nu}^*,k}$  (sometimes referred to as fast transmittance coefficients), a set of diverse atmospheric profiles is used to compute, for each profile and for several viewing angles, accurate LBL transmittances for each level defined in the atmospheric pressure layer grid. The convolved level-to-space transmittances  $\hat{\tau}_{j,\bar{\nu}^*}$  are then used to compute the  $a_{j,\bar{\nu}^*,k}$  coefficients by linear regression of  $\hat{\sigma}_{j,\bar{\nu}^*} - \hat{\sigma}_{j-1,\bar{\nu}^*}$ , or equivalently

$$-\ln\left(\frac{\hat{\tau}_{j,\bar{\nu}^*}}{\hat{\tau}_{j-1,\bar{\nu}^*}}\right) \quad (4)$$

versus the predictor values calculated from the profile variables for each profile at each viewing angle.

For each gas allowed to vary, the profiles used to compute the database of LBL transmittances are chosen to represent the range of variations in temperature and absorber amount found in the real atmosphere. In this paper only H<sub>2</sub>O and O<sub>3</sub> are allowed to vary, the others are held constant and will be referred to as fixed. The water vapour and fixed gas fast transmittance coefficients were derived by use of a training set of 42 profiles. To derive the regression coefficients for ozone, 33 profiles were used.

The database of LBL transmittances was generated by using GENLN2 (Edwards, 1992), a general-purpose LBL atmospheric transmittance and radiance model. The line parameters were obtained from the 1996 edition of the HITRAN molecular database (Rothman et al., 1998). Fixed gases are defined as CO<sub>2</sub>, N<sub>2</sub>O, CO, N<sub>2</sub>, CH<sub>4</sub>, O<sub>2</sub>, CFC11, and CFC12. For all these constituents tropospheric climatological concentrations estimated for the year 2005 were used. Continuum type absorption for H<sub>2</sub>O, N<sub>2</sub> and CO<sub>2</sub> was included in the computations using the semiempirical approach of Clough et al. (1989) (CKD version 2.1) as well as line-mixing effects for CO<sub>2</sub> using coefficients from Strow et al. (1994). Transmittances were computed from 0.005 hPa to each of the 43 standard pressure levels, at 0.001 cm<sup>-1</sup> resolution for each atmospheric profile and six viewing angles, namely, the angles for which the secant has equally spaced values from 1 to 2.25.

Once the LBL transmittances were integrated over the channel spectral responses, they were used to compute three sets of regression coefficients because the fast model treats separately the absorption by the fixed gases, water vapour, and ozone. Since the convolution of the transmittance of all the gases differs from the product of the transmittance of the single gases convolved individually, the monochromatic transmittance approximation

$$\hat{\tau}_{\bar{\nu}^*,j}^{tot} = \hat{\tau}_{\bar{\nu}^*,j}^{fix} \hat{\tau}_{\bar{\nu}^*,j}^{wv} \hat{\tau}_{\bar{\nu}^*,j}^{oz} \quad (5)$$

where  $\hat{\tau}_{\bar{\nu}^*,j}^{tot}$  is the convolved transmittance of all the gases and  $\hat{\tau}_{\bar{\nu}^*,j}^{fix}$ ,  $\hat{\tau}_{\bar{\nu}^*,j}^{wv}$ , and  $\hat{\tau}_{\bar{\nu}^*,j}^{oz}$  are the transmittances of the single gases convolved individually, might not be accurate because, for example, absorption by water vapour is not totally uncorrelated with absorption by the fixed gases. To reduce the



errors introduced by separation of the gas transmittances after convolution, the total model transmittance is written as:

$$\hat{\tau}_{\tilde{\nu}^*,j}^{tot} = \hat{\tau}_{\tilde{\nu}^*,j}^{fix} \frac{\hat{\tau}_{\tilde{\nu}^*,j}^{fix+ww}}{\hat{\tau}_{\tilde{\nu}^*,j}^{fix}} \frac{\hat{\tau}_{\tilde{\nu}^*,j}^{fix+ww+oz}}{\hat{\tau}_{\tilde{\nu}^*,j}^{f+ww}} \quad (6)$$

where the superscripts denote what was included in the LBL computations and the three terms on the right hand side of Eq. (3) are what is predicted by the fast model. Since all the terms but  $\hat{\tau}_{\tilde{\nu}^*,j}^{fix+ww+oz}$  cancel, the correct total convolved transmittance is left. Note that in the formulation of RTIASI,  $\hat{L}_{j,\tilde{\nu}^*}^u$  (Eq. 2) is defined as

$$\hat{L}_{j,\tilde{\nu}^*}^u = [B_{\tilde{\nu}^*}(\tilde{T}_j)] (\hat{\tau}_{j,\tilde{\nu}^*} - \hat{\tau}_{j-1,\tilde{\nu}^*}) \quad (7)$$

where  $\tilde{T}_j$  is a scene temperature defined as the layer mean temperature obtained by use of the Curtis-Godson air density weighted mean value. Equation 2 is based on the assumption that the mean radiance from a layer can be given by averaging the profile variables at the top and the bottom of the layer. This is a reasonable approximation if the atmosphere is divided up into enough layers so that the assumption of homogeneity within a layer is valid. Trials have shown that mean layer quantities obtained by dividing the atmosphere into the 43 layers used in RTAIRS can significantly differ if Eq (2) is used instead of Eq. (7). However, use of Eq(7) implies the computation of the scene temperature  $\tilde{T}_j$  and this degrades significantly the execution time of the adjoint routines. Since in an operational environment execution time is a major issue, Eq (2) is used instead.

## 2.2 The fast transmittance model

The functional dependence of the predictors  $X_{j,k}$  used to parameterise the optical depth  $\hat{\sigma}_{\tilde{\nu}^*,j}$  depends mainly on factors such as the absorbing gas, spectral response function and spectral region although the order in which the gases are separated out (Eq. 6) and the layer thickness can also be important. The model predictors used in this paper are listed in Table 1 whereas the profile variables are defined in Table 2.

Within the framework of a linear regression method, the great variability between extreme profiles makes the regression prone to numerical instabilities and thus difficulties in calculating the coefficients can arise if the predictors are allowed to vary too much. To avoid these difficulties predictors in this paper are defined by taking the ratio with respect to the values for a reference profile (see table 2).

Since most of the absorption in the temperature sounding channels is due to gases whose concentration is held fixed, transmittances for these channels are less difficult to model in that for a given viewing angle the transmittance depends only on the temperature profile. For water vapour and ozone sounding channels the variation in absorber amount has to be taken into account. The fast transmittance model predicts the polychromatic transmittance defined in Eq. 4. One can give a model to compute transmittances based on the assumption that the basic behaviour of the quantity defined in Eq.5 is that of the layer optical depth for a gas



in a homogeneous layer at pressure  $p(l)$ , temperature  $T(l)$  an absorber amount  $n(l)$ . A set of basic predictors can then be defined based on simple functions of the viewing angle and of the profile variables (all defined in table 2) in the layer  $j$ ,  $T_r(j)$ ,  $W_r(j)$ ,  $O_r(j)$  and  $\delta T(j)$ . One can expect the layer optical depth to be proportional to  $n$  for weak absorption and  $\sqrt{n}$  for strong absorption (Goody and Yung, 1989). The absorption due to the combined effect of weak and strong lines can be obtained using an intermediate value of the exponent. This was accounted for by introducing a term proportional to  $\sqrt[4]{n}$ . Values of the exponent greater than 1 can be introduced to account for effects of higher order. For the variable species the slowly varying dependence on temperature was modelled by scaling the terms proportional to  $n$  and  $\sqrt{n}$  with a  $\delta T(j)$  factor. For water vapour only it was found beneficial to introduce a  $|\delta T(j)| \delta T(j)$  factor to scale the term proportional to  $n$ . The angular dependence was addressed by scaling the layer amount through the secant of the viewing angle. As discussed above, for a fixed viewing angle the transmittance for the temperature channels depends only on the temperature profile. For these channels the most basic predictors are drawn on the ratio  $T_r(j)$ . First and second order terms were included. The inclusion of terms that depend only on the viewing angle had also to be envisaged since the effect of a variable viewing angle is to slightly alter and to impart an offset to the curve that represents the variation of optical depth with temperature. For water vapour the contribution of the continuum type absorption is of particular importance. The self-continuum contributes to absorption for most of the AIRS channels and is predominant in the window regions. It displays a dependence on the inverse of the temperature and is proportional to the square of water amount. The foreign-continuum is only important at wave numbers greater than  $1250 \text{ cm}^{-1}$ . It displays a weaker dependence on temperature than the self-continuum and is linearly proportional to the water amount. Both effects are included in the water model. This is an improvement to the approach followed in RTIASI where no predictors for the continuum were included. Since we are predicting polychromatic transmittances, adjustment terms must be included to extend the validity of the model from monochromatic to polychromatic transmittances. In fact account must be taken for the dependence of the layer transmittance on the properties of the atmosphere above the layer. Despite the fact that Eq. 5 reduces this dependence, the layer transmittance for two profiles having the same layer temperature but different temperature profiles over the actual layer will nevertheless differ in that the profile with greater optical depth above the layer will have smaller optical depth within the layer. This effect can be modelled by introducing predictors representative of the effective temperature and species column density above the layer. Those used in this paper are based on the ones given by Fleming and McMillin (1977) and their form was arrived at empirically by trial and error. These are predictors  $T_w(j)$ ,  $W_w(j)$  and  $O_w(j)$  in Table 2. The different form of the predictors used for the ozone and water model reflects the different order in which the gases are separated out in Eq. (6).

RTAIRS features a revised set of predictors for ozone that are different from the ones used in RTIASI. This has lead to a significant enhancement of the capability of the fast model to reproduce the LBL transmittances. The most basic monochromatic-type predictors were not changed. Instead the terms with



forms such as  $\frac{\int O(p) dp}{\int O^*(p) dp}$  were dropped and predictors  $X_{10,j}$  and  $X_{11,j}$  were added to improve prediction

of the ozone transmittance for large viewing angles.

### 2.3 Weighting of the input data prior to the regression

The scheme used in RTIASI to model the behaviour of the water vapour layer optical depth involves a split algorithm. Two sets of regression coefficients are computed to model the absorption in the optically thin and optically thick regimes. The use of the split algorithm means that a running sum must be maintained in the fast transmittance model to use the appropriate regression coefficients (see Matricardi and Saunders, 1999). This can result in discontinuities in the water vapour Jacobians. To eliminate these discontinuities, a single algorithm for water vapour is used in RTAIRS with the data being weighted prior to performing the regression. In fact, since the radiance coming either from the layers where no attenuation is taking place or from the layers where the transmittance has become very small contributes little to the total radiance, not all the data are of equal importance for the regression. To improve the accuracy of the regression it would be desirable to have the computation of the regression coefficients not to be influenced by data corresponding to optically thick situations. These data have a negligible impact on the simulated radiances and exhibit behaviour that is more complex to model than the one for the optically thin case. In RTAIRS the following approach is adopted: data are weighted in terms of the effective contribution to the total radiance with the weighting function chosen to be the partial derivative of the layer optical depth with respect to the top of atmosphere radiance. The process of computing weighted regression coefficients is iterative and can be described as follows: firstly, regression coefficients are computed setting the weighting function equal to 1. Although at this stage the accuracy of the regression coefficients is negatively influenced by data points corresponding to optically thick situations, this allows for a preliminary weighting function to be computed using the gradient of the fast radiative transfer model. Regression coefficients can now be generated weighting the data prior to regression. Since the preliminary weighting function was obtained based on unweighted data points, the weighted regression coefficients are used to compute an updated weighting function that in turn is used to derive a further set of weighted regression coefficients. This process can be iterated for a number of times but in practice it was found that after two iterations the impact on the computation of the top of the atmosphere radiance of regression coefficients generated using an updated weighting function was a negligible fraction of the instrument noise.

## 3 PERFORMANCE OF THE FAST MODEL FOR AIRS SIMULATIONS

The accuracy of the fast model can be assessed by a comparison of the transmittances and radiances computed by the fast model with the corresponding values from LBL models in different ways. Firstly the fast model transmittance profiles and top of the atmosphere radiances computed for the dependent set of profiles used to train the fast model can be compared with the LBL model equivalents to determine the accuracy of the fast model itself. Secondly a set of profiles independent of the regression coefficients can be used to allow uncertainties from different type of profiles to be included. Thirdly an independent set of profiles can be used to validate the fast model radiances with a different LBL model to allow spectroscopic and other uncertainties to be included in the validation.



The comparison of transmittances is more useful to understand how the model performs and to see where it needs to be improved, but the comparison of radiances is the most important as the radiances are what will be used. The analysis of the results discussed below concentrates on the error of the RTAIRS in terms of the bias, standard deviation and root mean square (rms) of the radiance and transmittance differences between the fast and LBL radiative transfer models. Validation against a different LBL model was not part of this exercise. Note that spectroscopic errors in the LBL models are not addressed here.

### 3.1 Results for the dependent set of profiles

The simulation of the layer optical depth using Eq. 1 is the essence of a regression based fast radiative transfer model. For the temperature and water vapour sounding channels of AIRS, the dependent set of fast model transmittances computed using GENLN2 for the 43 water vapour profiles and six scan angles from  $0^\circ$  to  $64^\circ$  were compared to the LBL equivalents. A similar comparison was made for the ozone-sounding channels using LBL transmittances for the 34 ozone profiles. Results are shown in Figures 1 and 2 where the maximum value of the rms of the difference between fast model and LBL layer-to-space transmittances is plotted for the water vapour and ozone profiles respectively. Biases are typically less than 10% of the standard deviations. Maximum errors are generally found near the peak of the weighting functions. Water vapour channels are the more difficult to model. Best results are obtained for those channels for which absorption is mostly due to fixed gases and whose weighting function peaks very high above the surface. Figure 2 displays the performance of the revised predictors for ozone. There is an almost universal improvement, more than halving the rms in the strong 9.8 : m band.

Errors in brightness temperature were computed by using the fast model transmittances as compared with those computed by using the LBL transmittances in Eq. 1. For the channels of the AIRS the Planck function does not vary significantly over the channel response so that in Eq. 1 it can be represented by the Planck function evaluated at the central frequency of the channel without introducing any significant error. Results for the dependent 43 profile set and six viewing angles are shown in figures 3 and 4 where the bias and standard deviation of the difference between the fast and LBL computed radiances in units of equivalent black body brightness temperature is given. It should be noted that a constant climatological ozone profile is used for this set so that no conclusions can be drawn on the performance of the ozone channels. Biases are typically less than 0.03 K (absolute value) whereas standard deviations are less than 0.2 K with more than 98% of the channels displaying standard deviations less than 0.15K. The largest source of error comes from the water vapour model but, in general, the transmittance model fits the regression profiles very well. More insight can be gained by comparing the rms error in radiance units with the radiance noise of the AIRS instrument. This is given in figure 5 where the ratio of the rms error to the instrument noise is plotted. Only those channels for which the noise is well characterised are shown. The error exceeds the noise only for a very small fraction of the channels.

The fitting errors of the fast transmittance model for ozone can be translated into brightness temperature errors using the same approach followed for the 43-profile set. The 34 ozone profile set is now used. Only the ozone transmittance is predicted by the model. The water vapour and fixed gas transmittances are those computed by the LBL model. Results are shown in figure 6 where the standard deviation of the error is shown. Values are typically less than 0.1 K that is more than one half the error obtained by use of the old ozone predictors. Biases are ten times smaller than standard deviations.



### 3.2 Results for the independent set of profiles

A complete validation of the fast model requires the use of an independent set of profiles. The sampling strategy described by Chevalier et al. (2000) was used for the sampling of profiles generated from the ECMWF atmospheric model. The 13766 initial profiles were randomly sampled to select a subset of 176 profiles to be used in the training/testing of the fast radiative transfer model. The dataset used in this paper comprises 117 profiles since the profiles with low surface pressures (less than 950 hPa) were not included. For those profiles whose surface pressure is greater than 950 hPa but less than 1013.25 hPa, the temperature and specific humidity are extrapolated to the surface assuming adiabatic expansion. Note that while temperature and specific humidity profiles are from the ECMWF model, ozone was added separately from the Fortuin and Langematz climatology (1994) depending on season and latitude. The dataset was designed to cover a wide range of temperature and water vapour profiles, which usually do not exceed the extremes included in the dependent set. All profiles of temperature, water vapour and ozone were interpolated on to the 43 standard pressure levels used by the fast model and an independent set of LBL transmittances was computed for the six different viewing angles using the methods described in section 2.

Uncertainties from profiles different from those used to train the fast model result in a degradation of the performance of the water vapour and ozone model. Figure 7 shows the maximum value of the rms of the difference between fast model and LBL transmittances. Higher values of the rms are observed for the water vapour channels whose weighting functions peaks well above the surface and for the ozone channels in the strong 9.8 : m band. Slightly higher values of the rms can also be seen in the window regions. A key feature to note is that the bias is now giving an important contribution to the rms. In the case of the 9.8 : m ozone band the contribution of the bias to the rms is predominant. For the other channel the bias is now three times higher than the values displayed in the dependent set case. As before, these results can be translated into brightness temperature errors. Figures 8, 9 and 10 show the bias, standard deviation and signal-to-noise ratio for the independent set. The ozone channels display a large negative bias in the 9.8 : m band. The small negative bias around  $730 \text{ cm}^{-1}$  must also be attributed to the ozone transmittance model. No significant differences are observed for the temperature sounding channels whereas for the strong water vapour band a largely positive bias is now displayed whose order of magnitude is typically three times the largely negative bias displayed in the dependent set case. In the window regions the bias is now marginally higher. In terms of standard deviation the degradation of the performance in the temperature sounding and window region is only marginal. The worst results are achieved for the high peaking water vapour channels. Although the maximum values are largely unchanged, the minimum values are now typically three times higher than those displayed in the dependent set case. It is interesting to note that for the ozone channels the standard deviation has been greatly reduced. In fact the bias is now predominating for these channels. Note that the use of the revised ozone predictors has resulted in an rms error that is typically three times less than that resulting from use of the old predictors. Also of note is the reduction of the error in the window region due to the introduction of the water vapour continuum dedicated predictors. This is shown in figures 11 and 12 where the rms error resulting from the use for the old and revised predictors is displayed respectively. The worst performance for the high peaking water vapour channels can be tentatively explained by the fact that the fast model was not properly trained. The water vapour profiles between 300 and 100 hPa were in fact obtained by extrapolating the 300 hPa value to the 100 hPa value using a cubic law (Matricardi and Saunders, 1999). This might have resulted in a behaviour that is not observed in the dependent profile set and that the fast model may find difficult to reproduce. No clear explanation can be given for the behaviour displayed by the



ozone channels even though the fact that the ozone profiles in the independent set are not thermodynamically linked to the temperature profiles might have artificially degraded the results.

As expected, the error-to-noise ratio for the independent set has raised above the values displayed for the dependent set. This is shown in Fig. 10. The error-to-noise ratio is now above 1 for a large portion of the ozone and water vapour channels. It should be noted however that in terms of brightness temperatures the rms error for the independent set is largely below 0.25 K that is still below the errors introduced by uncertainties in the spectroscopic parameters used to calculate the LBL transmittances (Rizzi et al. 2001).

### 3. PERFORMANCE OF THE FAST MODEL FOR SIMULATIONS OF ATOVS AND METEOSAT RADIANCES

The set of predictors developed for RTAIRS was implemented into the RTTOV-5 scheme in an effort to improve prediction of the HIRS channels. The basic assumptions made in section 2 (b) are still valid. Because of the wider response function one might expect some departure from the behaviour in the polychromatic regime but in general there is no reason of principle why the performance of the transmittance model should deteriorate when applied to the HIRS channels.

As demonstrated in Saunders et al. (1999), RTTOV-5 errors for the window (7-8, 13), water vapour (11,12) and ozone (9) channels exceed the noise equivalent temperatures (Ne) T) values. Most importantly, the error introduced by the transmittance model can be a significant fraction of the error introduced by uncertainties in the spectroscopic parameters used in the LBL computations. There is obviously room for improvement for the simulation of these channels.

The transmittance model of RTTOV-5 is described in Eyre and Wolf (1988) and Eyre (1991). Recent developments can be found in Saunders et al. (1999). In RTTOV-5 the optical depth for a homogeneous layer is approximated by the low-order terms of a multivariate Taylor expansion about a reference profile. The optical depth can then be written using Eq. 3 where the predictors are now drawn from the differences  $\delta T(j)$  (Table 2) and  $\delta n(j) = n(j) - n^r(j)$  where  $n^r(j)$  is the absorber amount for the reference profile. The model is then extended to polychromatic transmittances by introducing predictors representative of the effective temperature and specie column density above the layer. Since predictors are drawn from departures from the reference profile, the water vapour predictors can vary by order of magnitudes between extreme profiles. As observed before this makes difficult to compute coefficients using a linear regression scheme. To avoid these difficulties, the basic predictors are scaled through different functions of a variable that varies directly with the precipitable water across the layer. The form of the scaling variable was arrived at empirically. This results in a new set of predictors that falls in two groups: one that is intended to cover the strong absorption limit and one that is intended to cover the weak absorption limit. Note that the predictors introduced to extend the validity of the model to polychromatic transmittances are now incorporated either into the first or second group. There are no terms proportional to  $\sqrt[4]{n}$  and the form of the predictors that include quantities averaged above the layer differ significantly from those used in RTAIRS where, for example, an inverse dependency on the pressure weighted water vapour column density above the layer is introduced. The model for ozone uses the same predictors as used for water vapour and there are no predictors to model the water vapour continuum type absorption.



### 3.1 Results for the dependent set of profiles

(i) *Comparison of model radiances and transmittances for ATOVS channels.* A comparison similar to the one described in section 3 was made for the channels of the HIRS instruments by comparing the operational and modified fast model transmittances and radiances to the LBL model equivalents. The 43-profile set was used for water vapour and fixed gas transmittances whereas the 34-profile set was used for ozone. Comparisons were made for six viewing angles from  $0^{\text{B}}$  to  $64^{\text{B}}$ . Results are given for the HIRS channels of NOAA-14. They can be generalised to the HIRS channels of NOAA-15 and NOAA-16 since very slight differences were observed.

The maximum value of biases and standard deviations of difference between fast model and LBL computed NOAA-14 HIRS (1-19) level-to-space transmittances are given in table 3. Table 3 points to a significant and universal improvement when the new model is used. For both operational and improved fast model the bias is generally less than the standard deviation. Best results are for those channels where the absorption is mostly due to fixed gases. Water vapour channels are still the more difficult to model. Scores are improved at all pressure levels (although not shown in the table) and in absolute terms they are most dramatic for channels 8 through 12. This is displayed in figure 13 and 14 where the rms of the difference between fast model and LBL computed transmittances is shown for the operational and improved model respectively. Maximum errors are found near the peaks of the weighting functions. At some pressure levels the rms error for the water vapour channels has been reduced by an order of magnitude. For the ozone and window channel a typical five-fold reduction of the rms error has been achieved.

The ability of the fast model to reproduce the LBL radiances in terms of the bias and standard deviation of the difference between the fast model and LBL computed radiances is given in table 4. Radiances are in units of equivalent black body brightness temperature. Errors in brightness temperature were computed by using the fast model transmittances as compared with those computed by using the LBL transmittances in Eq. 1. Radiances for all 6 viewing angles are included in the statistics. For HIRS channels 9 the model simulates only the ozone transmittance. For this channel water vapour and fixed gas transmittances are taken to be the LBL ones. For the other channels transmittances for a constant climatological profile are used for ozone. Results are shown for the operational and improved model. Also shown is the signal-to-noise ratio obtained as the ratio of the rms error in radiance units to the instrument radiance noise. As for table 3, table 4 points to a universal improvement when the new predictors are used. For both models, biases are typically less than the standard deviation. However, for the operational model, channel 12 displays a bias that is a significant fraction of the standard deviation. The improved model is virtually unbiased to the LBL. Standard deviations for the temperature sounding channels are marginally improved (for the operational model errors were already well below the noise). A dramatic reduction of the error has been achieved for the other channels. For the window channels HIRS-8 and HIRS-19 the standard deviation has been reduced by an order of magnitude. For the lower tropospheric water vapour channels HIRS-10 and HIRS-11 and for the ozone channel HIRS-9 a five-fold reduction of the standard deviation has been achieved. Note that the rms error for the HIRS-12 upper tropospheric water vapour channel has been reduced from 0.7K to 0.1K. These results are depicted at a glance in figure 15 where the rms error for the operational and improved model is shown for the HIRS channels of NOAA-14, NOAA-15 and NOAA-16. Slightly different values of the score between different platforms must be attributed to modification of the spectral response functions.

For the improved model the signal-to-noise ratio is significantly below 1 for all channels. For the operational model the signal exceeds the noise for channels HIRS-9, HIRS-10 and HIRS-19 with the same quantity being very close to 1 for channels HIRS-8 and HIRS-11.

(ii) *Comparison of model radiances for METEOSAT channels.* Radiances from the Meteosat Visible and Infrared Radiation Imager (MVIRI) instrument on board the European Organisation for Exploitation of Meteorological Satellites (EUMETSAT) Geosynchronous Meteorological Satellite (METEOSAT) are monitored routinely at ECMWF. The accuracy of radiance simulation of the MVIRI water vapour channels is of particular relevance in that this can help understand the origin of large systematic differences between observed and measured radiances. The performance of the operational and improved fast model was assessed for the window and water vapour channels of MVIRI applying the methods described in the previous section. Results for three different platforms are given in table 5 where the bias and standard deviation of the difference between the fast model and LBL computed brightness temperatures for the dependent 43 profile set and six viewing angles is shown. Results for the MVIRI channels mirror those obtained for the HIRS channels. Scores are improved for both window and water vapour channel. Biases and standard deviations are now typically an order of magnitude lower than the ones achieved by the operational fast model. Differences between platforms are negligible.

### 3.2 Results for the independent set of profiles

Results for the transmittances of ATOVS channels are given in table 6 where the maximum value of biases and standard deviations of the difference between fast model and LBL computed transmittances are shown. Use of the independent profile results in a degradation of the scores for both operational and improved fast model. The improved fast model is again performing better than the operational one. As for the dependent set case, improvements were made at all pressure levels. Figures given in section 3(a) regarding the reduction of the rms error made at the various pressure levels are still valid. Note that the relative variation of the standard deviation is roughly the same for both models whereas the relative variation of the bias is larger for the improved model. In fact for this model the bias is now a significant fraction of the standard deviation (but it is still much lower than the operational model bias). For example channel HIRS-9 displays an absolute bias as large as the standard deviation.

Results in terms of brightness temperature differences are shown in Table 7. Increments to the values obtained for the dependent set case are in general larger for the operational model. To note is the significantly better accuracy achieved by use of the new predictors for the ozone channel HIRS-9, the window channels HIRS-8 and HIRS-19 and the water vapour channels HIRS-10, HIRS-11 and HIRS-12. In particular for the water vapour channels HIRS-11 and HIRS-12 the standard deviation has been reduced six-fold. For the improved model the signal-to-noise ratio is still significantly below one for all channels. Channels HIRS-8, HIRS-9, HIRS-10, HIRS-11 and HIRS-19 display a signal-to-noise ratio larger than 1 when the operational predictors are used.

In general the introduction of uncertainties from the use of different type profiles has not resulted in a dramatic degradation of the performance of the improved model. Errors are still less than 0.13K and most importantly they are well below those introduced in the LBL computations by uncertainties in the spectroscopic data. Errors introduced by the parameterisation used in the operational model can instead add



significantly to the latter. Note that the improved predictors can be used to reproduce radiances for all the microwave instruments supported by RTTOV-5 to accuracy that is better or at the same level as the one that can be achieved by use of dedicated predictors in RTTOV-5.

### 3.3 Results for the independent LBL model

(i) *Comparison of model radiances for ATOVS channels.* The original set of 13766 sampled profiles (reduced to 8978 because profiles with surface pressure less than 950 hPa were excluded) used to derive the 117 independent profiles was used to compare fast model radiances with radiances computed using Synstrad, a radiative transfer model developed at EUMETSAT (Tjemkes and Schmetz, 1997). Synstrad is based on the radiance sampling method developed by Sneden et al. (1975) and can reproduce LBL radiances to 1) 2 % accuracy. It uses line parameters from the 1996 edition of the HITRAN database and the continuum type absorption for H<sub>2</sub>O, N<sub>2</sub> and CO<sub>2</sub> is parameterised using the semiempirical approach of Clough et al. (1989) (CKD version 2.2). For the fixed gases the concentrations were the same used in RTTOV-5. In this validation one allows for several uncertainties to be included in the validation. Typically, uncertainties result from the use of different types of profiles, from different forward model mechanics and from different spectroscopy used in the LBL computations. In this section, radiances computed by using convolved fast model transmittances in Eq.1 were compared with Synstrad LBL radiances obtained by convolving the channel response function with the monochromatic radiances computed using the monochromatic transmittances in Eq1. As observed in section 2(a), the use of convolved transmittances in Eq.1 is based on the assumption that the same equation written for monochromatic radiances still applies when integrated over the spectral response function of a satellite sounder channel. If the Planck function does not vary too much over the channel response function, it can be evaluated at the central frequency of the channels. This can be accurate for the narrow channels of the AIRS, but for the broad channels of the HIRS the concept of modified Planck function must be introduced that takes account of the averaging of the true Planck function over the spectral response of channel  $i$  for scene temperature  $T$ . The modified Planck function for channel  $i$  is given by

$$B_i(T) = \frac{c_{1,i}}{\exp\left(\frac{c_{2,i}}{a_i + b_i T}\right) - 1}$$

where  $c_{1,j} = c_1 \nu_i$  and  $c_{2,j} = c_2 \nu_i$  with  $c_1$  and  $c_2$  the Planck function constants and  $\nu_i$  the central frequency of the channel  $i$ .  $a_i$  and  $b_i$  are the so-called “band correction coefficients” (Weinreb et al. 1981) and are computed from the channel filter response. Prior to comparing fast model to Synstrad radiances a study was made to quantify the errors introduced by the use of the band correction coefficients in Eq.1. Radiances computed using GENLN2 LBL convolved transmittances in Eq.1 were compared to GENLN2 radiances obtained by convolving the channel response function with the monochromatic radiances computed using the monochromatic transmittances in Eq1. In both cases the term  $\hat{L}_{j,\tilde{\nu}}^u$  in Eq.1 was computed using Eq.7 and the scene temperature was defined as the Curtis-Godson air density weighted mean value in the layer. Since the same scene temperature was used, differences between radiances can only be attributed to errors introduced by the use of the approximated form of the radiative transfer equation. Computations were made for the 117 independent profiles. Only nadir view monochromatic radiances were generated. Results are



shown in table 8 where the bias and standard deviation of the difference between approximated and exact LBL radiances is shown for the channels of the HIRS instrument on board the NOAA-14, NOAA-15 and NOAA-16 satellites. Use of the approximate form of Eq.1 does not introduce any significant bias for most of the channels of NOAA-14. Channel HIRS-12 displays the larger value at  $-0.35$  K. Smaller values between  $-0.21$ K and  $-0.1$  K are observed for channels HIRS-15, HIRS-13 and HIRS-16. Standard deviations are in general smaller than biases. Results for NOAA-15 and NOAA-16 must be interpreted in the light of the fact that for some channels (i.e. HIRS-12 and HIRS-16) a different spectral response function has been adopted. For example, the new spectral response for channel HIRS-12 is located in a different region of the spectrum and the Full Width at Half Height (FWHH) is roughly one-half the old value. As a result of this, the bias for channel HIRS-16 has increased from  $-0.1$  to  $-0.17$  K whereas the bias for channel HIRS-12 is now between  $-0.0014$ K and  $-0.0044$ K. A larger bias of  $-0.21$  K is found for channel HIRS-15. Results for channel HIRS-12 are of particular interest in that they can help understanding of some of the differences observed in the fast model versus Synstrad comparison. Results for this exercise are given in Table 9 where the statistics of the difference between fast model and Synstrad generated radiances is shown for both the operational and improved fast models. Errors were computed for the 8978 profiles described above. Only radiances for the nadir looking case were generated. Spectral response functions for the channels HIRS-8, HIRS-9, HIRS10, HIRS-11 and HIRS-12 of NOAA-14 were considered. To compute the contribution due to the term  $\hat{L}_{j,\bar{v}}^u$ , Eq.2 was used for both fast and line-by-line model. For the channels included in this exercise, results are very similar to those obtained when only uncertainties from different types of profiles were included in the comparison (see table 7). This means that differences are likely to be dominated by errors in the fast transmittance scheme with differences between the two LBL models (GENLN2 and Synstrad) playing a less important role. For the improved model standard deviations are in general less than or of the same order as the biases. For channel HIRS-12 a larger bias is observed because of the inaccuracy introduced by use of the approximate form of Eq.1. In fact the value observed for the bias is very close to the one tabulated in table 8. For the other water vapour channels small differences between the values tabulated in tables 7 and 9 can be attributed to differences introduced by the LBL codes (for example water vapour continuum plays an important role for channel HIRS-10). For the operational model the standard deviations are typically larger than (for channel HIRS-12 significantly larger) or of the same order as the biases. The use of the new predictors result in a 3-to 4-fold reduction of the rms error. Maximum errors are also significantly reduced. For example the maximum error for channels HIRS-12 has been reduced from to 5.2K to 1.4K. Also to be noted is the performance for the window channel HIRS-8 that with the new predictors displays a maximum error of 0.2K to be compared to 0.94 K obtained with the old predictors. The behaviour of HIRS-9 has yet to be fully understood since the maximum error for the operational and improved fast model is virtually the same although the overall performance for the improved model is significantly better. Maximum errors for this channel are found for very dry and cold profiles.

A major negative feature of the operational fast model that has been corrected by the improved model is the dependence of the error on air mass type. This is illustrated in figures 16 and 17 where the error is plotted with the total water content in the profile. For the operational fast model the error steadily increases with the total water content and is most dramatic in channel HIRS-11 although is clearly visible also for the other channels. This should be compared with the behaviour of the improved model that displays no marked dependence of the error on the air mass type. Errors for this model are randomly distributed. Biases are likely



to be due differences between LBL models. The same behaviour (if not worse) is displayed when the error is plotted with the surface temperature or the latitude: the warmer and moister the profile, the larger the error for the operational model.

(ii) *Comparison of model radiances for the METEOSAT channels.* An exercise similar to the one described in the previous section was carried out for the channels of the MVIRI instrument on board the METEOSAT-7 satellite. Results are given in table 9. As for the HIRS channels, significant improvements were made using the new predictors. To note is the large bias observed in the water vapour channel. Although no trials were made for the MVIRI channels, the large width of the spectral response function of the water vapour channel is likely to introduce a large bias when the approximated for of the radiative transfer equation is used. Given the demonstrated skill of the fast transmittance algorithm it is reasonable to assume that for the improved model this contributes to a large fraction of the bias.

### 3.4 Comparison of Jacobians

As stated in the introduction, emphasis should put in the validation of fast model Jacobians since this is a fundamental quantity in the direct assimilation of satellite radiance in a NWP model. In this paper fast model Jacobians were compared to LBL generated Jacobians for the profiles selected in the study of Garand et al. (2001) and for the 8978 independent profiles used in section 3(b). Both assessments are described below.

(i) *Validation against GENLN2 computed Jacobians.* The GENLN2 Jacobians (obtained by the perturbation method) computed in Garand et al. (2001) were compared to the analytical Jacobians generated by the operational and improved fast model. The quality of fit measure,  $M$ , defined as

$$M = 100 \sqrt{\frac{\sum_{i=1}^N (J_{m,i} - J_{r,i})^2}{\sum_{i=1}^N J_{r,i}^2}} \quad (8)$$

where  $J_m$  and  $J_r$  are the model and reference Jacobian respectively and the sum is over the number of levels,  $N$ , was computed for five atmospheric profiles (independent of the regression coefficients) and for a selected number of HIRS channels of the NOAA-14 platform. Results for temperature, ozone and water vapour Jacobians are tabulated in Table 10. Among the profiles used in Garand et al., profiles with number from 7 to 18 are ranked by increasing mean atmospheric temperature, profiles 19-30 are ranked by increasing integrated water vapour and profiles 31-42 by increasing total ozone. Note that if the maximum value of the Jacobian is less than 0.005, no result is given since in that case the value of  $M$  is meaningless. The first noticeable feature is that for most of the considered cases the quality of fit for the improved model is at a level typical among LBL models ( $M \# 5$ ). For the temperature sounding channels HIRS-2, HIRS-5 and HRS-15 both models are able to reproduce the LBL temperature Jacobian to a high degree of accuracy ( $M \# 5$ ), the improved model performing better than the operational one for channels HIRS-5 and HIRS-15, slightly worse for channel HIRS-2. For the ozone channel HIRS-9 scores are significantly better when the improved model is used. The quality of fit for the temperature and ozone Jacobian has been dramatically improved ( $M \# 9.8$ ), in fact for most of the cases the quality of the fit obtained with the operational model is to be



considered fair to marginal (15#M#25). Because of the presence of ozone absorption lines, the ozone Jacobian is given for channel HIRS-5 as well. Despite the significantly better quality of the fit, the values of  $M$  are unusually high for the improved model. This can be partly explained by the fact that the sensitivity to ozone perturbation for this channel is very low and the maximum value of the Jacobian approaches the threshold value quoted above. For the water vapour channels HIRS-10, HIRS-11 and HIRS-12 the temperature and water vapour Jacobians computed using the improved model have the right shape and amplitude and peak at the right height. This results in very low values of the quality of fit measure  $M$  that never exceeds 8.7 and is for most of the cases smaller than 5 making the fast model Jacobians remarkably close to the LBL ones. Conversely the Jacobians generated by the operational model differ from the LBL ones in amplitude and shape and to some degree the peak position resulting in higher values of  $M$  that can be as big as 20. This is illustrated in figure 18 where the HIRS-12 water vapour Jacobian is plotted for profile 19. The amplitude peak is 20% off for the operational model and noticeable also is the kink between 250hPa and 100hPa for the operational model that is absent in the Jacobian generated by the improved model.

(ii) *Validation against GENLN2 computed Jacobians.* Synsatrad was used to compute using the perturbation method LBL Jacobians that were compared with the fast model generated Jacobians for the 8978 independent profiles used for the validation of fast model radiances. Due to the computational load for the LBL model, Jacobians were only generated for channels HIRS9, HIRS-12 of NOAA-14 and for the water vapour channel of METEOSAT-7. The average value of the quality of fit  $M$  is given in table 11 where results are tabulated for all the profiles and for Mid/High-Latitude and Tropical profiles only. Most noticeable is the dramatic improvement achieved by the improved model in the computation of temperature and water vapour Jacobian for the water vapour channel. Also significant is the improved quality of the fit for the ozone channel HIRS-9. For this channel use of the improved model has resulted in the elimination of a large wiggle observed in the operational model temperature Jacobian between 50 hPa and 350 hPa. Also note how for the improved model the quality of the fit depends only slightly on the air-mass type whereas larger variations are observed for the operational model. For both models, scores for the temperature Jacobian in channel HIRS-9 are better for the tropical profiles. For the Mid/High-Latitude case a degradation of the quality of the fit is observed although for the improved model the fit is still good.

#### 4 CONCLUSIONS

The forthcoming launch of AIRS, with a much higher spectral resolution than the existing HIRS radiometer, offers the exciting possibility of a significant improvement in the quality of information on meteorological parameters for use in NWP. At ECMWF a fast radiative transfer model has been developed for AIRS in preparation for exploitation of the AIRS data in an NWP model by use of a variational analysis scheme. The model fit to the LBL radiances shows a degree of accuracy such that errors from the fast transmittance algorithm do not add significantly to the errors that are likely to be introduced in the LBL by uncertainties in the spectroscopic data. Although performance of RTAIRS is considered adequate for this study some improvements could be made as we move towards the launch of the AIRS such as to allow some of the fixed gases to vary and to divide the atmosphere into a greater number of layers to improve the accuracy of the radiative transfer computations.

The set of predictors developed for RTAIRS was implemented into the RTTOV-5 scheme in an effort to improve prediction of the HIRS channels. With the new predictors a closer fit to the LBL radiances is



achieved for all the channels, the error being dramatically reduced for channel HIRS-8, HIRS-9, HIRS-10, HIRS-11 and, most significantly, HIRS-12. In particular, for the water vapour channels HIRS-11 and HIRS-12 a seven-fold reduction of the rms error was obtained. Similar results were found for the infra-red and water vapour channel of the MVIRI instrument on board the METEOSAT satellites. Comparison with LBL computed Jacobians show that Jacobians generated by the improved RTTOV-5 are remarkably close to the LBL ones. For most of the cases considered in the study the quality of the fit is at a level typical of LBL models. Conversely, Jacobians generated by the operational model differ from the LBL ones in amplitude and shape and to some degree the peak position. Comparison of the improved RTTOV-5 radiances with equivalent quantities computed using an independent LBL model for a large set of atmospheric profiles show that errors do not display any marked dependence on the air-mass type whereas for the operational model the warmer and moister the profile the larger the error. The RTTOV-5 with new predictors is also able to reproduce radiances for all the microwave sounders supported by RTTOV-5 to accuracy at or below the one achieved by use of dedicated predictors in the operational version of the model. This means that a single set of predictors can be used to accurately simulate radiances for a wide range of satellite instruments, from the conventional infrared and microwave to the advanced high-resolution sounders. As a result of this, a new version of RTTOV, RTTOV-7, has been jointly developed with Météo France and The Met Office that among the other new features includes the use of the new predictors and the possibility of supporting the AIRS instrument.

### Acknowledgements

The LBL computed Jacobians were provided by L. Garand (MSC, Canada). Roger Saunders (The Met Office, UK) provided the convolved transmittances for the HIRS channels. Discussions with J.N. Thépaut, A. McNally and G. Kelly, all staff at ECMWF, were also valuable during the course of this work.

### References:

- Aumann, H. H. and Pagano, R.J., 1994, "Atmospheric Infrared Sounder on the Earth Observing System", *Optical Engineering*, **33**, pp. 776-784.
- Chevalier, F., Chedin, A., Cheruy, N., and Morcrette, J.J., "TIGR-like atmospheric profile database for accurate radiative flux computation", *Q. J. R. Meteorol. Soc.*, **126**, pp. 777-785.
- Clough, S.A., Kneizys, F.X. and Davis, R.W., 1989, "Line shape and the water continuum:", *Atmos. Res.*, **23**, pp. 229-241.
- Edwards, D.P., 1992, "GENLN2. A general line-by-line atmospheric transmittance and radiance model", NCAR Technical note NCAR/TN-367+STR.
- Eyre, J.R. and Woolf, H., 1988, "Transmittance of atmospheric gases in the microwave region", *Appl. Opt.*, **27**, pp.3244-3249.



Eyre, J.R., 1991, "A fast radiative transfer model for satellite sounding system", ECMWF Research Department Technical memorandum 176 (European Centre for Medium-Range Weather Forecasts, Reading, UK).

Fortuin, J.P.F., and Langematz, U., "An update of the global ozone climatology and on current ozone and temperature trends," Proc. SPIE 2311, pp. 207-216 (1994).

Garand, L., Turner, D.S., Larocque, M., Bates, J., Boukabara, S., Brunel, P., Chevallier, F., Deblonde, G., Engelen, R., Hollingshead, M., Jackson, D., Kedlovec, G., Joiner, J., Kleespies, T., McKague, D.S., McMillin, L., Moncet, J.-L., Pardo, J.R., Rayer, P.J., Salathe, E., Saunders, R., Scott, N.A., Van Delst, P. and Woolf, H., 2001, "Radiance and jacobian intercomparison of radiative transfer models applied to HIRS and AMSU channels", in print, *J. Geophys. Res.*, **106**, 15 pp.

Hannon, S.E., Strow, L.L. and McMillan, W.W., 1996, "Atmospheric infrared fast transmittance models: a comparison of two approaches", in *Optical Spectroscopic Techniques and Instrumentation for Atmospheric and Space Research II*, P.B. Hays and J. Wang, eds., Proc. SPIE **2830**, pp. 94-105.

Matricardi, M. and Saunders, R., 1999, "Fast radiative transfer model for simulation of infrared atmospheric sounding interferometer radiances", *Applied Optics*, **38**, pp. 5679-5691.

Fleming, H.E. and McMillin, L., 1977, "Atmospheric transmittance of an absorbing gas. 2. A computationally fast and accurate transmittance model for slant paths at different zenith angles", *Appl. Opt.*, **16**, pp. 1366-1370.

McMillin, L.M., Fleming, H.E. and Hill, M.L., 1979, "Atmospheric transmittance of an absorbing gas. 3: A computationally fast and accurate transmittance model for absorbing gases with variable mixing ratios", *Appl. Opt.*, **18**, pp. 1600-1606.

Rabier, F., Thepaut, J. and Courtier, P., 1998, "Extended assimilation and forecast experiments with a four dimensional variational assimilation scheme", *Q. J. R. Meteorol. Soc.*, **124**, pp. 1861-1887.

Rizzi, R., Matricardi, M. and Miskolczi, F., 2001, "On the simulation of up-looking and down-looking high-resolution radiance spectra using two different radiative transfer models", Accepted for publication in *Applied Optics*.

Rothman, L.S., Rinsland, C.P., Goldman, A., Massie, S.T., Edwards, D.P., Flaud, J.-M., Perrin, A., Camy-Peyret, C., Dana, V., Mandin, J.-Y., Schroeder, J., McCann, A., Gamache, R.R., Watson, R.B., Yoshino, K., Chance, K.V., Jucks, K.W., Brown, L.R., Nemtchinov, V., and Varanasi, P., 1998, "The HITRAN molecular spectroscopic database and HAWKS (HITRAN Atmospheric Workstation): 1996 edition", *J. Quant. Spectrosc. Radiat. Transfer*, **60**, pp. 665-710.

Saunders, R., Matricardi, M. and Brunel, P., 1999, "A fast radiative transfer model for assimilation of satellite radiance observations – RTTOV-5", *ECMWF Research Department Technical Memorandum 282 (European Centre for Medium-Range Weather Forecasts, Reading, UK, 1999)*



Snedden, C, Johnson, H. and Krupp, B., 1975, "A statistical method for trating molecular line opacities", *Astrophys. J.*, **204**, pp. 281-289.

Strow, L.L., Tobin, D.C. and Hannon, S.E., 1994, "A compilation of First-Order Line\_Mixing coefficients for CO2 Q-branches", *J. Quant. Spectroscop. Radiat. Transfer*, **52**, pp. 281-294.

Susskind, J., Rosenfeld, J. and Reuter, D., 1983, "An accurate radiative transfer model for use in the direct physical inversion of HIRS2 and MSU temperature sounding data", *J. Geophys. Res.*, **88**, pp.8850-8568.

Tjemkes, S.A. and Schmetz, J., 1997, "Synthetic satellite radiances using the radiance sampling method", *J. Geophys. Res.*, **102D**, pp. 1807-1818.

Weinreb, M.P., Fleming, H.E., McMillin, L.M. and Neuendorffer, A.C., 1981, "Transmittances for the TIROS Operational Vertical Sounder", NOAA Tech. Rep. NESS 85.



Predictor	Fixed gases	Water vapour	Ozone
$X_{j,1}$	$\sec(\theta)$	$\sec^2(\theta) W_r^2(j)$	$\sec(\theta) O_r(j)$
$X_{j,2}$	$\sec^2(\theta)$	$(\sec(\theta) W_w(j))^2$	$\sqrt{\sec(\theta) O_r(j)}$
$X_{j,3}$	$\sec(\theta) T_r(j)$	$(\sec(\theta) W_w(j))^4$	$\sec(\theta) O_r(j) \delta T(j)$
$X_{j,4}$	$\sec(\theta) T_r^2(j)$	$\sec(\theta) W_r(j) \delta T(j)$	$(\sec(\theta) O_r(j))^2$
$X_{j,5}$	$T_r(j)$	$\sqrt{\sec(\theta) W_r(j)}$	$\sqrt{\sec(\theta) O_r(j)} \delta T(j)$
$X_{j,6}$	$T_r^2(j)$	${}^4\sqrt{\sec(\theta) W_r(j)}$	$\sec(\theta) O_r(j)^2 O_w(j)$
$X_{j,7}$	$\sec(\theta) T_w(j)$	$\sec(\theta) W_r(j)$	$\frac{O_r(j)}{O_w(j)} \sqrt{\sec(\theta) O_r(j)}$
$X_{j,8}$	$\sec(\theta) \frac{T_w(j)}{T_r(j)}$	$(\sec(\theta) W_r(j))^3$	$\sec(\theta) O_r(j) O_w(j)$
$X_{j,9}$	$\sqrt{\sec(\theta)}$	$(\sec(\theta) W_r(j))^4$	$O_r(j) \sec(\theta) \sqrt{(O_w(j) \sec(\theta))}$
$X_{j,10}$	$\sqrt{\sec(\theta)} {}^4\sqrt{T_w(j)}$	$\sec(\theta) W_r(j) \delta T(j)  \delta T(j) $	$\sec(\theta) O_w(j)$
$X_{j,11}$	0	$(\sqrt{\sec(\theta) W_r(j)}) \delta T(j)$	$(\sec(\theta) O_w(j))^2$
$X_{j,12}$	0	$\frac{(\sec(\theta) W_r(j))^2}{W_w}$	0
$X_{j,13}$	0	$\frac{\sqrt{(\sec(\theta) W_r(j) W_r(j))}}{W_w(j)}$	0
$X_{j,14}$	0	$\sec(\theta) \frac{W_r^2(j)}{T_r(j)}$	0
$X_{j,15}$	0	$\sec(\theta) \frac{W_r^2(j)}{T_r^4(j)}$	0

Table 1. Predictors used by RTAIRS for Fixed Gases, Water Vapour and Ozone



$$T(l) = [T^{profile}(l+1) + T^{profile}(l)] / 2 \quad T^*(l) = [T^{reference}(l+1) + T^{reference}(l)] / 2$$

$$W(l) = [W^{profile}(l+1) + W^{profile}(l)] / 2 \quad W^*(l) = [W^{reference}(l+1) + W^{reference}(l)] / 2$$

$$O(l) = [O^{profile}(l+1) + O^{profile}(l)] / 2 \quad O^*(l) = [O^{reference}(l+1) + O^{reference}(l)] / 2$$

$$P(l) = [Pres(l+1) + Pres(l)] / 2$$

$$T_r(l) = T(l) / T^*(l) \quad \delta T(l) = T(l) - T^*(l) \quad W_r(l) = W(l) / W^*(l)$$

$$O_r(l) = O(l) / O^*(l)$$

$$T_w(l) = \sum_{i=2}^l P(i) [P(i) - P(i-1)] T_r(i-1)$$

$$W_w(l) = \{ \sum_{i=1}^l P(i) [P(i) - P(i-1)] W(i) \} / \{ \sum_{i=1}^l P(i) [P(i) - P(i-1)] W^*(i) \}$$

$$O_w(l) = \{ \sum_{i=1}^l P(i) [P(i) - P(i-1)] O(i) \} / \{ \sum_{i=1}^l P(i) [P(i) - P(i-1)] O^*(i) \}$$

The  $Pres(l)$ 's are the values of the pressure at each level.  $T^{profile}(l)$ ,  $W^{profile}(l)$  and  $O^{profile}(l)$  are the temperature, water vapour mixing ratio and ozone mixing ratio profiles.  $T^{reference}(l)$ ,  $W^{reference}(l)$  and  $O^{reference}(l)$  are corresponding reference profiles. For these variables  $l$  refers to the  $l$ th level; otherwise  $l$  is the  $l$ th layer, i.e. the layer above the  $l$ th level. Note that we take  $P(0) = 2P(1) - P(2)$  and  $T_w(1) = 0$ .

Table 2. Definition of profile variables used in predictors defined in Table 1.



Channel number (NOAA-14 Central frequency (cm <sup>-1</sup> ))	Operational RTTOV Dependent set		Improved RTTOV Dependent set	
	Max Bias	Max Sdev	Max Bias	Max Sdev
1 (669)	0.00044	0.00097	-0.00001	0.00088
2 (679)	0.00041	0.00086	-0.00000	0.00047
3 (690)	0.00044	0.00089	-0.00000	0.00058
4 (704)	0.00050	0.00117	0.00004	0.00093
5 (714)	0.00063	0.00169	0.00004	0.00111
6 (733)	0.00425	0.00141	-0.00006	0.00082
7 (750)	-0.00149	0.00408	0.00009	0.00177
8 (899)	-0.00248	0.00657	0.00009	0.00062
9 (1028)	0.00055	0.00599	-0.00003	0.00139
10 (796)	-0.00354	0.00966	0.00004	0.00224
11 (1361)	-0.00348	0.01472	0.00024	0.00365
12 (1481)	-0.00889	0.02042	0.00059	0.00698
13 (2191)	0.00030	0.00109	-0.00003	0.00056
14 (2207)	0.00027	0.00059	-0.00001	0.00032
15 (2236)	0.00039	0.00088	-0.00001	0.00061
16 (2268)	0.00040	0.00101	0.00000	0.00069
17 (2420)	0.00008	0.00045	0.00000	0.00041
18 (2512)	-0.00840	0.00048	0.00000	0.00035
19 (2648)	-0.00115	0.00584	0.00000	0.00108

Table 3. Maximum value of biases and standard deviations of difference between line-by-line and fast model computed NOAA-14 HIRS (1-19) transmittances for a dependent set of 43 diverse profiles and six viewing angles.



Channel Number (NOAA-14 Central wave-number (cm <sup>-1</sup> ))	Operational RTTOV Dependent set			Improved RTTOV Dependent set		
	Bias (K)	Sdev (K)	S/N	Bias (K)	Sdev (K)	S/N
1 (669)	-0.01843	0.03745	0.01476	-0.00436	0.03754	0.01386
2 (679)	-0.01188	0.02487	0.03947	-0.00262	0.01860	0.02620
3 (690)	-0.00404	0.01617	0.03152	0.00086	0.01890	0.03639
4 (704)	0.01781	0.04078	0.13075	0.00420	0.0310	0.09506
5 (714)	0.02346	0.05674	0.29889	0.00198	0.04343	0.20708
6 (733)	0.01304	0.05334	0.27129	-0.001399	0.03235	0.15329
7 (750)	0.00238	0.08596	0.57233	-0.000799	0.04693	0.29563
8 (899)	-0.00829	0.06143	0.97289	-0.000272	0.00677	0.10720
9 (1028)	-0.02478	0.31693	1.71288	-0.001287	0.06408	0.40738
10 (796)	-0.01740	0.13365	1.35797	-0.001374	0.03609	0.36169
11 (1361)	-0.02863	0.43073	0.82410	0.00891	0.09033	0.17941
12 (1481)	-0.21603	0.64406	0.61894	0.00885	0.10333	0.09553
13 (2191)	0.00948	0.03791	0.32073	-0.000824	0.01693	0.13415
14 (2207)	0.01272	0.03052	0.32423	0.00002	0.01641	0.17078
15 (2236)	0.01872	0.03896	0.15945	-0.001177	0.02341	0.07555
16 (2268)	0.00442	0.05039	0.14575	0.00048	0.04060	0.08586
17 (2420)	0.00299	0.01029	0.17683	0.00095	0.00908	0.14912
18 (2512)	0.00018	0.00433	0.07491	0.00036	0.00331	0.05434
19 (2648)	-0.00527	0.06289	1.48548	-0.000339	0.00664	0.14955

Table 4. Biases and standard deviation of difference between line-by-line and fast model computed NOAA-14 HIRS (1-19) brightness temperatures for the dependent profile set. Also listed is the signal-to-noise ratio.



Channel number (METEOSAT 5 central frequency ( $\text{cm}^{-1}$ ))	Operational fast model Dependent set		Improved fast model Dependent set	
	Bias (K)	Sdev (K)	Bias(K)	Sdev(K)
1 (1597)	-0.09913	0.58787	0.00019	0.05941
2 (879)	-0.05700	0.08089	-0.00030	0.01036
<b>Channel number (METEOSAT 6 central frequency (<math>\text{cm}^{-1}</math>))</b>				
1 (1597)	-0.097012	0.58718	0.00117	0.05765
2 (875)	-0.057262	0.08192	-0.00035	0.01058
<b>Channel number (METEOSAT 7 central frequency (<math>\text{cm}^{-1}</math>))</b>				
1 (1577)	-0.091281	0.61139	0.00511	0.06899
2 (867)	-0.057428	0.08383	-0.00031	0.01240

Table 5. Biases and standard deviation of difference between line-by-line and fast model computed brightness temperatures for the dependent profile set.



Channel number (NOAA-14 Central frequency (cm <sup>-1</sup> ))	Operational RTTOV Independent set		Improved RTTOV Independent set	
	Max Bias	Max Sdev	Max Bias	Max Sdev
1 (669)	0.00068	0.00174	0.00070	0.00178
2 (679)	0.00082	0.00119	0.00038	0.00054
3 (690)	0.00080	0.00120	0.00038	0.00057
4 (704)	0.00099	0.00154	0.00046	0.00079
5 (714)	0.00124	0.00190	0.00063	0.00086
6 (733)	0.00092	0.00222	0.00056	0.00107
7 (750)	-0.00178	0.00470	0.00039	0.00181
8 (899)	-0.00173	0.00782	-0.00040	0.00108
9 (1028)	-0.00173	0.00612	0.00248	0.00286
10 (796)	-0.00436	0.01020	-0.00095	0.00301
11 (1361)	0.00272	0.01735	-0.00174	0.00678
12 (1481)	0.00365	0.02647	-0.00148	0.00989
13 (2191)	0.00040	0.001742	0.00011	0.00061
14 (2207)	0.00049	0.000709	0.00018	0.00034
15 (2236)	0.00059	0.000877	0.00036	0.00056
16 (2268)	0.00075	0.00106	0.00044	0.00071
17 (2420)	0.00049	0.00075	0.00037	0.00057
18 (2512)	0.00018	0.00066	0.00014	0.00032
19 (2648)	-0.00258	0.00686	0.00053	0.00218

Table 6. Maximum value of biases and standard deviations of difference between line-by-line and fast model computed NOAA-14 HIRS (1-19) transmittances for an independent set of 117 diverse profiles and six viewing angles.



Channel Number (NOAA-14 Central wave-number (cm <sup>-1</sup> ))	Operational RTTOV Independent set			Improved RTTOV Independent set		
	Bias (K)	Sdev (K)	S/N	Bias (K)	Sdev (K)	S/N
1 (669)	0.01706	0.03924	0.01476	-0.00215	0.02926	0.01026
2 (679)	0.02761	0.02897	0.05453	-0.01222	0.01404	0.02477
3 (690)	0.01738	0.02268	0.05014	-0.00597	0.01184	0.02342
4 (704)	-0.02435	0.04883	0.14789	0.01178	0.02401	0.07849
5 (714)	0.02346	0.06602	0.34181	0.02472	0.03299	0.20304
6 (733)	-0.02445	0.05774	0.31813	0.01094	0.03012	0.15862
7 (750)	0.00260	0.09991	0.69818	0.00312	0.04935	0.32834
8 (899)	0.02187	0.10196	1.65274	-0.00535	0.01482	0.24425
9 (1028)	-0.12630	0.32984	2.36406	0.09952	0.08255	0.86106
10 (796)	0.06772	0.19606	2.17149	-0.02193	0.05700	0.62730
11 (1361)	-0.17190	0.49649	1.09667	-0.03306	0.08965	0.20686
12 (1481)	-0.12927	0.81170	0.91626	-0.03747	0.13175	0.16051
13 (2191)	0.00178	0.04976	0.49130	0.00462	0.01914	0.17186
14 (2207)	-0.02070	0.04069	0.43827	0.00957	0.01657	0.21128
15 (2236)	-0.04258	0.04245	0.21194	0.01346	0.01751	0.07619
16 (2268)	-0.01885	0.02288	0.03676	0.01018	0.01722	0.02541
17 (2420)	-0.01349	0.01365	0.35488	0.00897	0.01114	0.26369
18 (2512)	-0.00304	0.00648	0.13597	0.00238	0.00354	0.07158
19 (2648)	0.02675	0.07602	2.06854	0.00431	0.02370	0.59991

Table 7. Biases and standard deviation of difference between line-by-line and fast model computed NOAA-14 HIRS (1-19) brightness temperatures for the independent profile set. Also listed is the signal-to-noise ratio.



NOAA-14			NOAA-15			NOAA-16		
Channel number (Central wave-number (cm-1))	Bias(K)	Sdev(K)	Channel number (Central wave-number (cm-1))	Bias(K)	Sdev(K)	Channel number (Central wave-number (cm-1))	Bias(K)	Sdev(K)
1 (669)	-0.0407	0.0115	1 (669)	0.0235	0.0143	1 (669)	-0.0878	0.0271
2 (679)	-0.0095	0.0037	2 (679)	-0.0126	0.0046	2 (679)	-0.0109	0.0054
3 (690)	0.0061	0.0044	3 (690)	0.0047	0.0041	3 (691)	0.0083	0.0046
4 (704)	0.0322	0.0088	4 (703)	0.0310	0.0085	4 (701)	0.0277	0.0088
5 (714)	-0.0005	0.0052	5 (716)	0.0058	0.0043	5 (716)	0.0066	0.0050
6 (733)	0.0038	0.0015	6 (732)	0.0027	0.0013	6 (731)	-0.0021	0.0019
7 (750)	0.0181	0.0051	7 (748)	0.0188	0.0049	7 (749)	0.0165	0.0069
8 (899)	0.0009	0.0004	8 (897)	0.0017	0.0008	8 (895)	0.0082	0.0025
9 (1028)	-0.0485	0.0092	9 (1032)	-0.0116	0.0034	9 (1032)	-0.0123	0.0036
10 (796)	0.0044	0.0008	10 (801)	0.0029	0.0011	10 (803)	0.0015	0.0017
11 (1361)	-0.0157	0.0361	11 (1362)	-0.0201	0.0326	11 (1362)	-0.0225	0.0322
12 (1481)	-0.3567	0.0542	12 (1530)	-0.0014	0.0060	12 (1525)	-0.0044	0.0064
13 (2191)	-0.1319	0.0195	13 (2188)	-0.1519	0.0230	13 (2184)	-0.1522	0.0239
14 (2207)	-0.0921	0.0122	14 (2210)	-0.0690	0.0091	14 (2206)	-0.1031	0.0140
15 (2236)	-0.2173	0.0408	15 (2235)	-0.2161	0.0392	15 (2234)	-0.2193	0.0385
16 (2268)	-0.1069	0.0606	16 (2242)	-0.1840	0.0413	16 (2244)	-0.1731	0.0398
17 (2420)	0.0400	0.0083	17 (2419)	0.0513	0.0105	17 (2415)	0.0604	0.0115
18 (2512)	0.0089	0.0025	18 (2519)	-0.0037	0.0014	18 (2516)	-0.0009	0.0143
19 (2648)	0.0101	0.0110	19 (2657)	0.0004	0.0067	19 (2664)	-0.0144	0.0138

Table 8. Biases and standard deviations of the difference between line-by-line radiances computed using convolved transmittances and line-by-line radiances obtained by convolving the channel spectral response function with the radiance computed using monochromatic transmittances.



NOAA-14 Channel Number	Operational model				Improved Model			
	Bias (K)	Sdev (K)	Rms (K)	Max Value (K)	Bias (K)	Sdev (K)	Rms (K)	Max Value (K)
8	-0.156	0.107	0.189	0.942	-0.077	0.029	0.082	0.203
9	0.324	0.258	0.414	1.969	0.078	0.153	0.171	1.991
10	-0.055	0.207	0.214	1.001	0.112	0.072	0.133	0.458
11	0.396	0.517	0.652	1.841	0.113	0.103	0.153	0.526
11	0.184	0.858	0.878	5.252	-0.261	0.118	0.287	1.410
METEOSAT-7 Channel number	Operational model				Improved Model			
	Bias (K)	Sdev (K)	Rms (K)	Max Value (K)	Bias (K)	Sdev (K)	Rms (K)	Max Value (K)
1	-0.406	0.932	1.017	-6.045	-0.726	0.168	0.745	-2.044
2	-0.302	0.138	0.332	-1.183	-0.120	0.035	0.125	-0.331

Table 9. Statistics of the difference between fast model and Synstrad generated radiances in HIRS and MVIRI channels for the 8978 profile independent set.



Operational Model													
Profile	T H-2	T H-5	O <sub>3</sub> H-5	T H-9	H <sub>2</sub> O H-9	O <sub>3</sub> H-9	T H-10	H <sub>2</sub> O H-10	T H-11	H <sub>2</sub> O H-11	T H-12	H <sub>2</sub> O H-12	T H-15
6	2.3	4.1	23.4	17.8	7.9	11.2	8.7	7.1	9.5	12.2	7.7	17.2	2.7
18	2.4	2.7	22.0	27.0	12.2	23.2	5.8	18.9	4.7	16.5	12.2	20.2	2.7
19	2.7	4.5	-----	8.7	-----	19.8	6.3	-----	12.6	10.0	13.5	16.6	3.4
30	2.4	4.2	26.8	10.4	3.1	25.0	8.8	11.5	7.8	17.0	18.5	13.4	2.7
31	2.7	3.9	-----	11.2	-----	9.7	-----	-----	9.5	15.8	10.2	18.0	4.4
Improved Model													
Profile	T H-2	T H-5	O <sub>3</sub> H-5	T H-9	H <sub>2</sub> O H-9	O <sub>3</sub> H-9	T H-10	H <sub>2</sub> O H-10	T H-11	H <sub>2</sub> O H-11	T H-12	H <sub>2</sub> O H-12	T H-15
6	2.7	2.5	15.2	7.2	3.1	4.6	6.5	3.0	3.1	3.6	1.5	2.0	2.3
18	2.7	2.7	8.4	8.7	1.6	5.2	3.9	3.7	2.1	3.2	3.8	4.2	2.3
19	2.9	2.4	-----	2.7	-----	5.9	6.4	-----	3.6	8.7	2.9	4.6	3.2
30	2.7	2.3	8.3	4.3	1.7	5.8	2.7	2.8	3.0	6.4	7.0	6.8	2.1
31	3.1	2.5	-----	4.6	-----	9.8	-----	-----	3.21	7.5	2.2	6.0	4.3

Table 10. Quality of fit measure F (no units) for temperature (T), ozone (O<sub>3</sub>) or water vapour (H<sub>2</sub>O) Jacobians for 5 independent atmospheric profiles in selected HIRS channels. Reference line-by-line Jacobians were obtained using GENLN2.



Operational model						
Profile	T H-9	O <sub>3</sub> H-9	T H-12	H <sub>2</sub> O H-12	T M-1	H <sub>2</sub> O M-1
<b>All</b>	19.531	14.413	17.395	30.727	17.237	31.204
<b>Mid/High-Latitude</b>	22.365	11.332	16.268	24.070	16.193	24.161
<b>Tropical</b>	16.212	18.021	18.715	38.521	18.461	39.448

Improved model						
Profile	T H-9	O <sub>3</sub> H-9	T H-12	H <sub>2</sub> O H-12	T M-1	H <sub>2</sub> O M-1
<b>All</b>	12.034	6.312	2.578	7.315	4.302	7.493
<b>Mid/High-Latitude</b>	15.806	5.918	2.708	7.703	4.341	7.837
<b>Tropical</b>	7.617	6.772	2.426	6.861	4.256	7.090

Table 11. *Quality of fit measure F (no units) for temperature (T), water vapour (H<sub>2</sub>O) or ozone (O<sub>3</sub>) Jacobians in channels HIRS-9, HIRS-12 and METEOSAT water vapour channel. Reference line-by-line Jacobians were obtained using Symsatrad.*

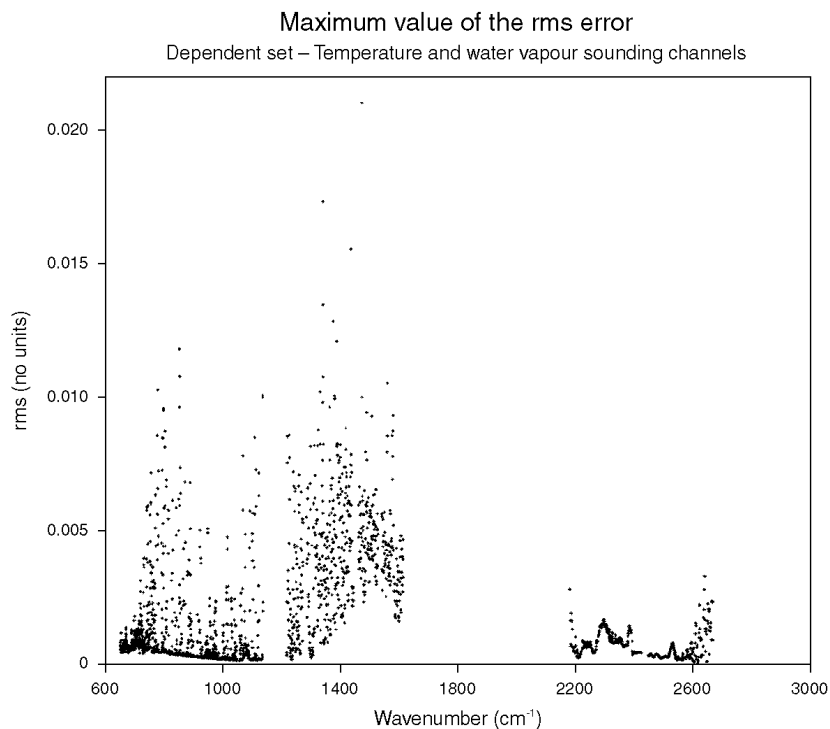


Fig 1. Maximum value of root mean square of difference between fast model and GENLN2 layer to top of atmosphere transmittances for AIRS for 43 diverse water vapour profiles and 6 viewing angles.

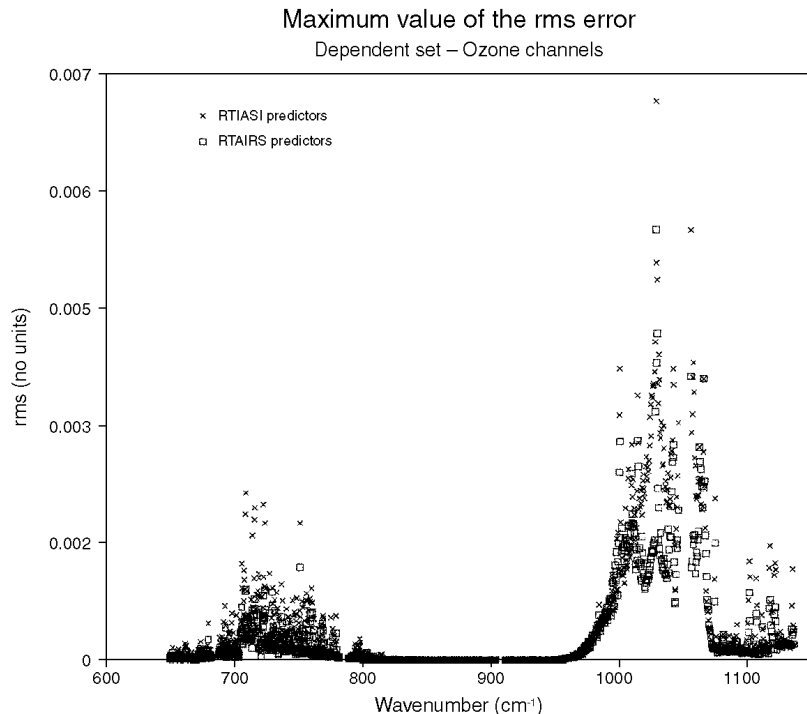


Fig 2. Maximum value of root mean square of difference between fast model and GENLN2 layer to top of atmosphere transmittances for AIRS for 34 diverse ozone profiles and 6 viewing angles. Results are shown for the transmittance model used in RTIASI and for the improved model used in RTAIRS.

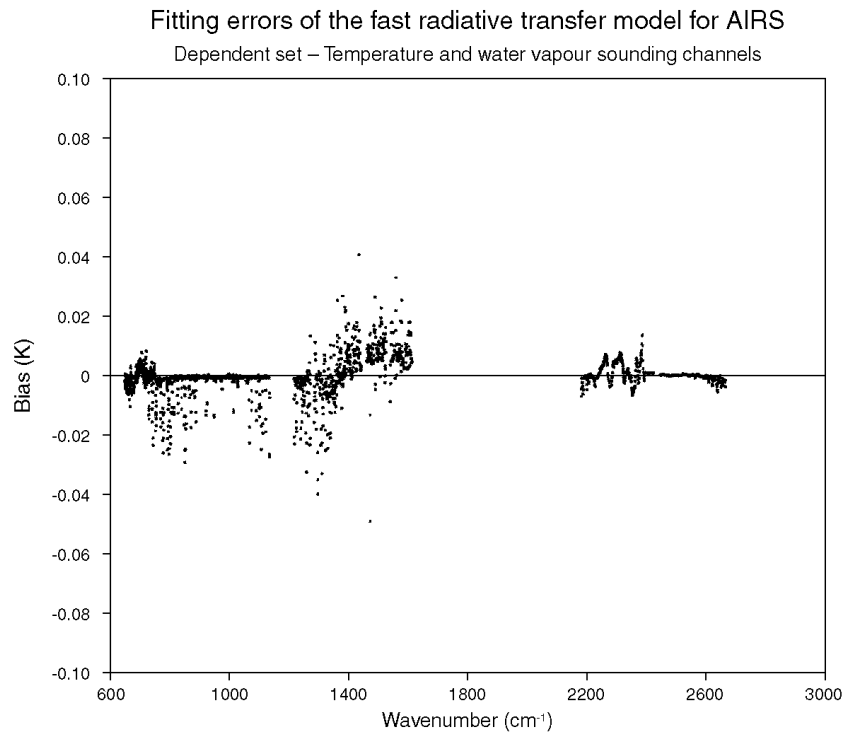


Fig 3. Mean value of the difference (bias) between fast model and GENLN2 computed brightness temperatures for AIRS for 43 diverse water vapour profiles and 6 viewing angles.

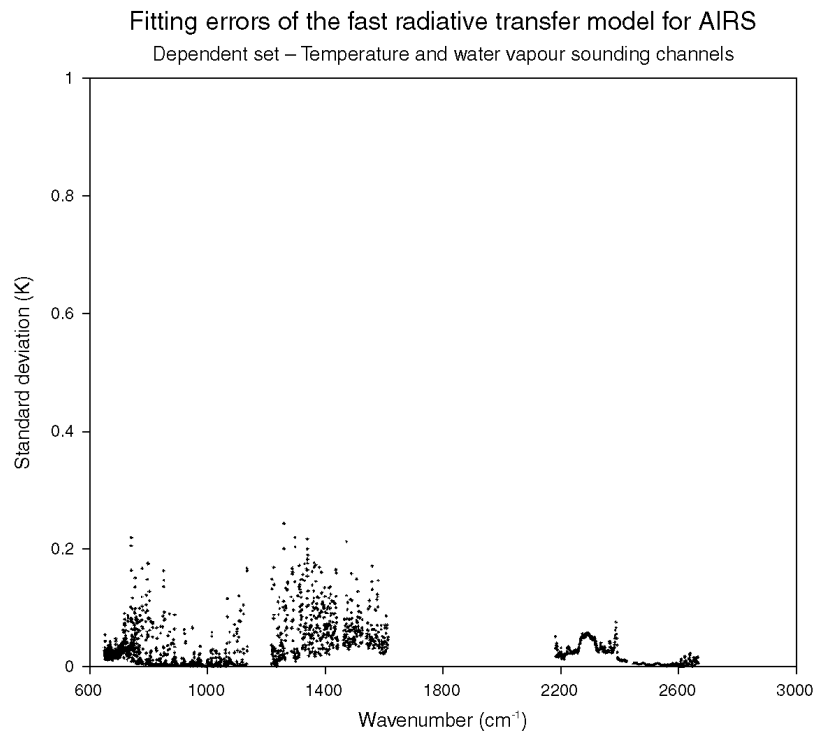


Fig 4. Standard deviation of the difference between fast model and GENLN2 computed brightness temperatures for AIRS for 43 diverse water vapour profiles and 6 viewing angles.

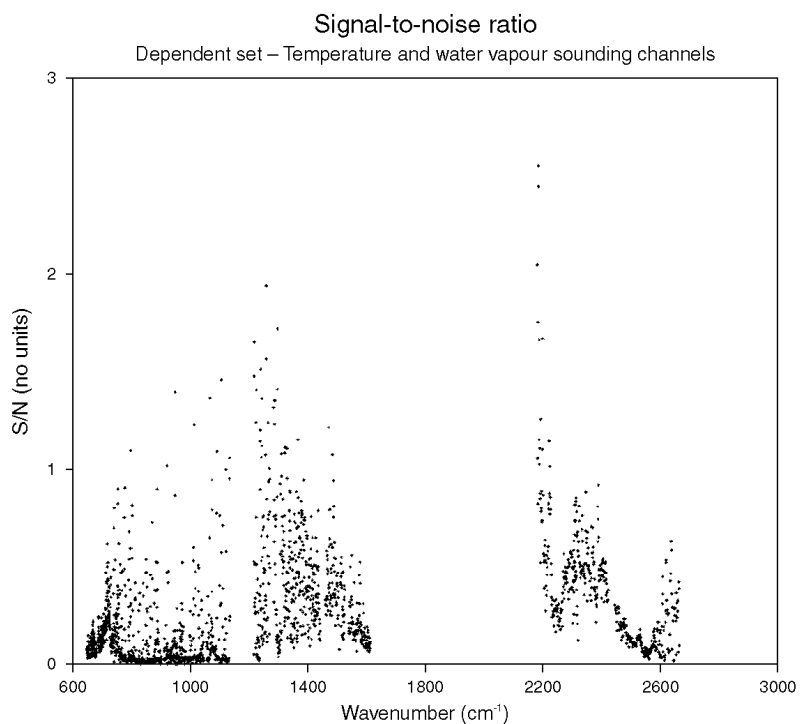


Fig 5. Signal to noise ratio for the AIRS channels for 43 diverse water vapour profiles and 6 viewing angles.

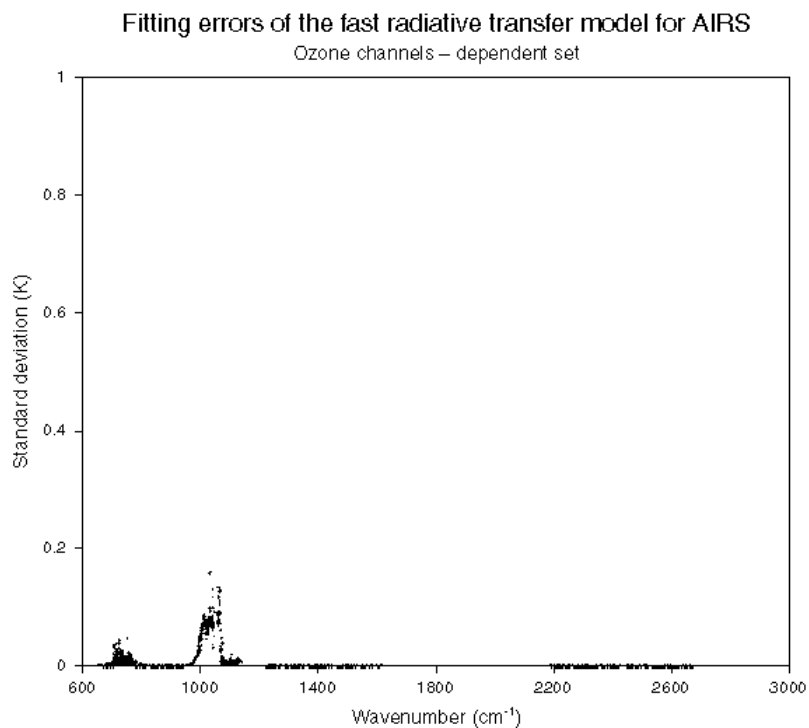


Fig 6. Standard deviation of the difference between fast model and GENLN2 computed brightness temperatures for AIRS for 34 diverse ozone profiles and 6 viewing angles.

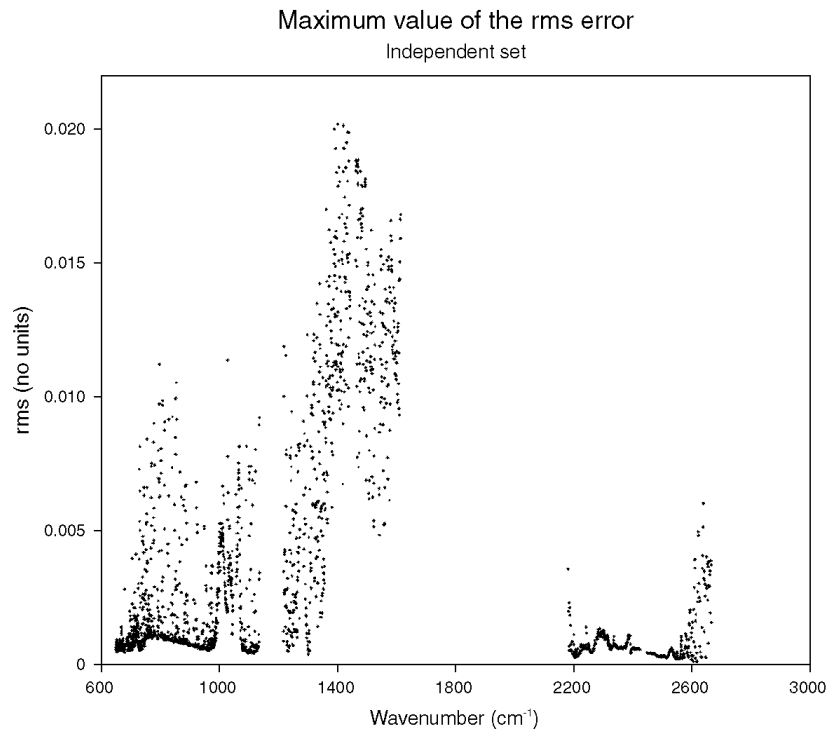


Fig 7. Maximum value of root mean square of difference between fast model and GENLN2 layer to top of atmosphere transmittances for AIRS for 117 independent profiles and 6 viewing angles.

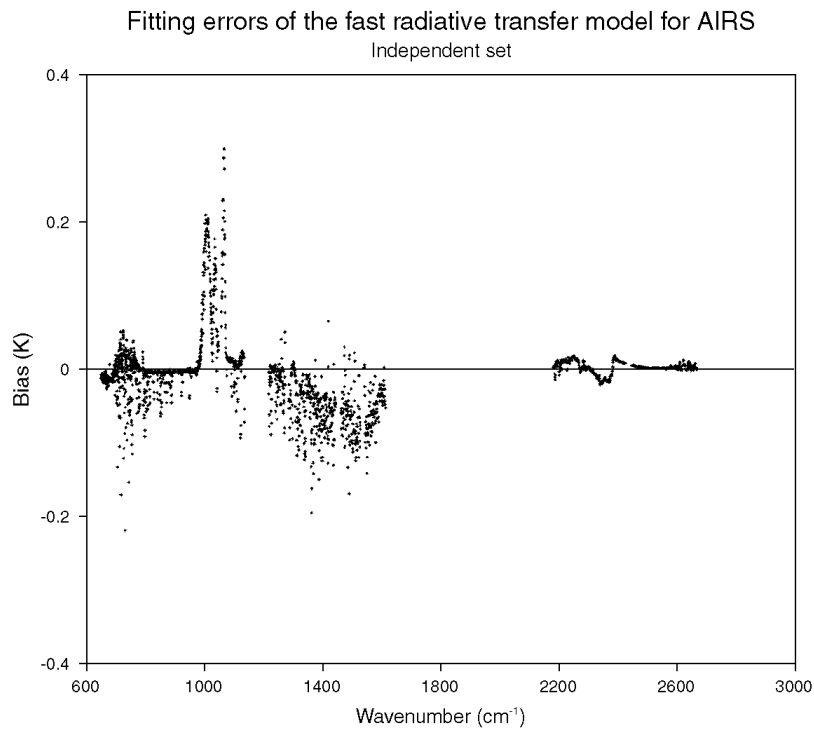


Fig 8. Mean value of the difference (bias) between fast model and GENLN2 computed brightness temperatures for AIRS for 117 independent profiles and 6 viewing angles.

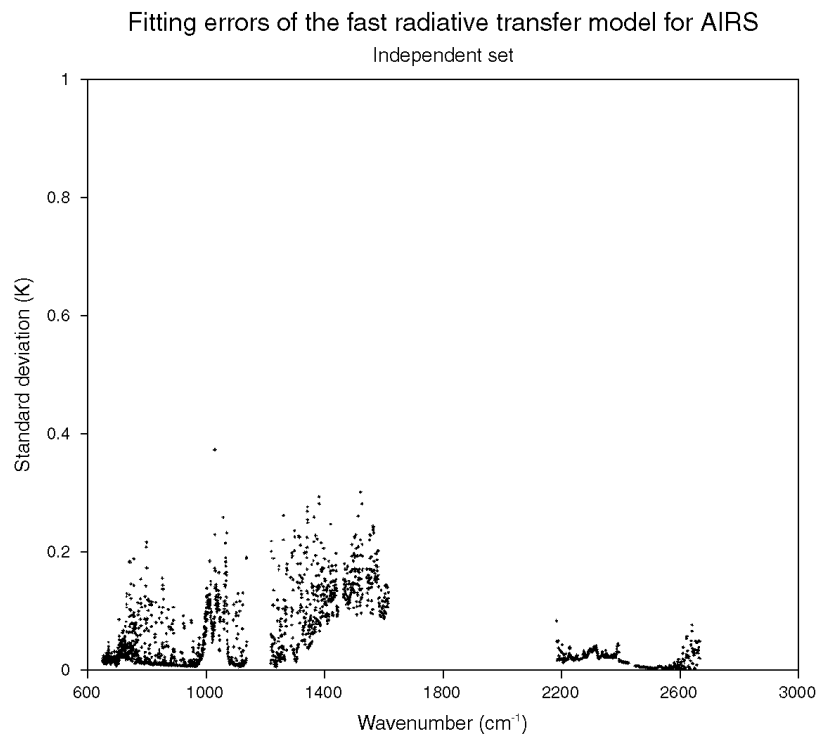


Fig 9. Standard deviation of the difference between fast model and GENLN2 computed brightness temperatures for AIRS for 117 independent profiles and 6 viewing angles.

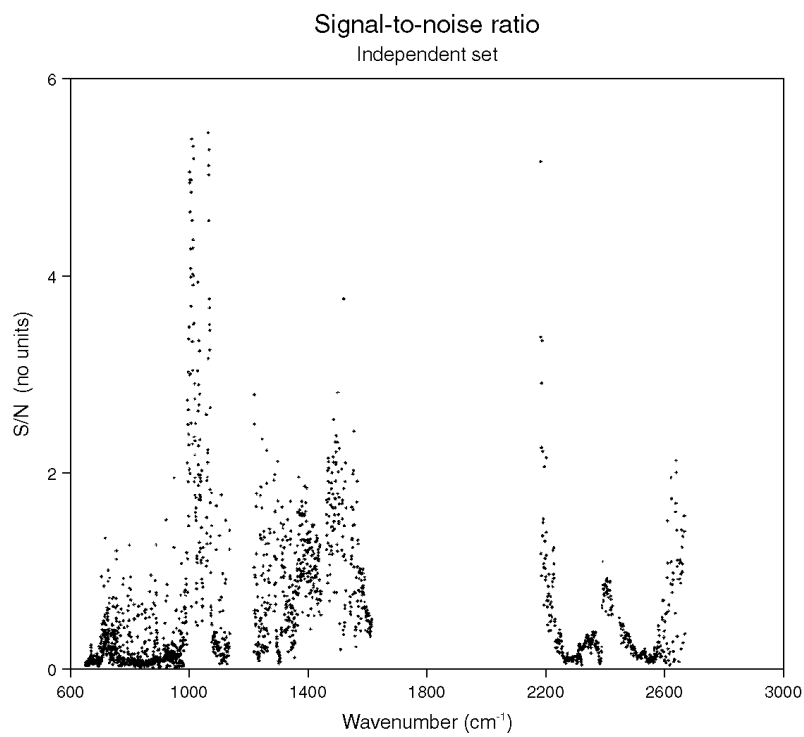


Fig 10. Signal to noise ratio for the AIRS channels for 117 independent profiles and 6 viewing angles.

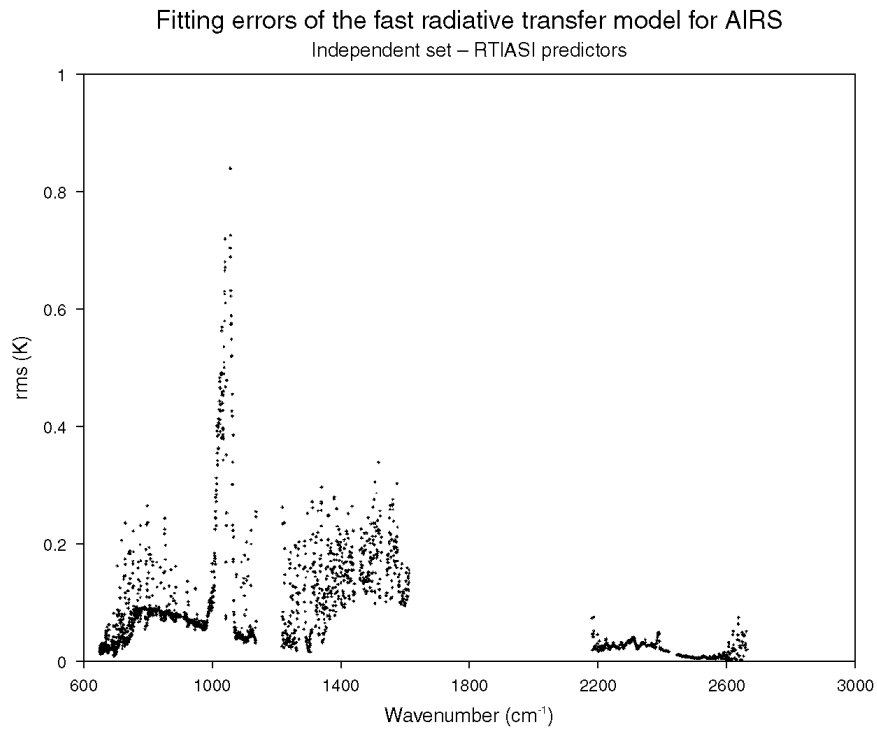


Fig 11. Root mean square of the difference between fast model and GENLN2 computed brightness temperatures for AIRS for 117 independent profiles and 6 viewing angles. Results are shown for the transmittance model used in RTIASI.

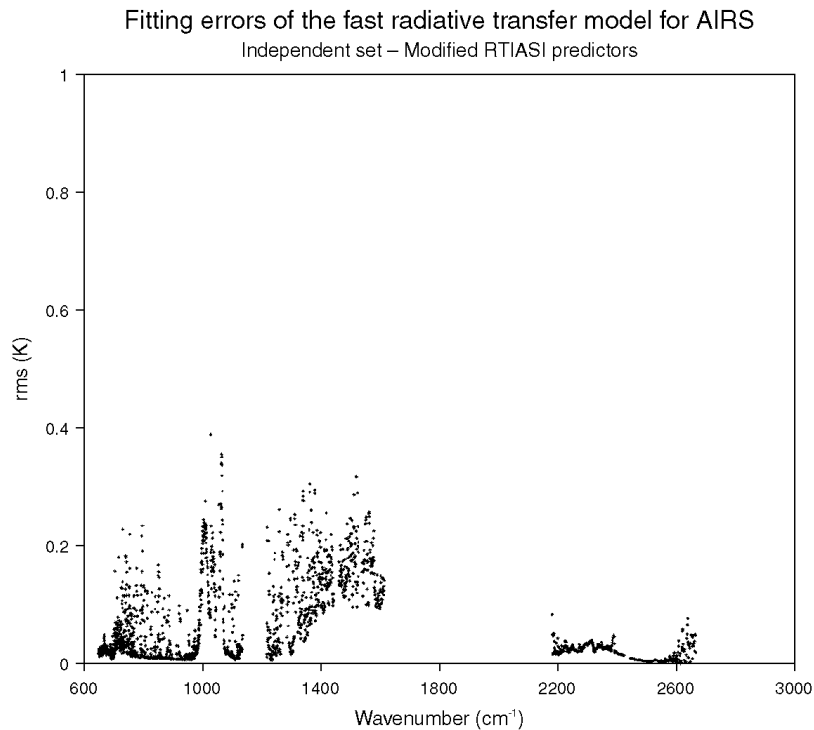


Fig 12. Root mean square of the difference between fast model and GENLN2 computed brightness temperatures for AIRS for 117 independent profiles and 6 viewing angles. Results are shown for the improved transmittance model used in RTAIRS.

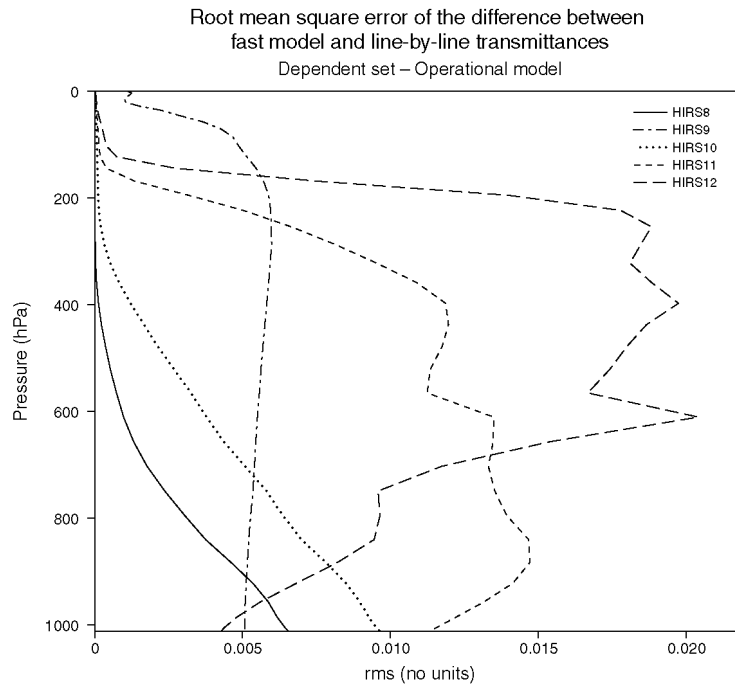


Fig 13. Root mean square of the difference between RTTOV-5 and GENLN2 HIRS channels 8, 9, 10, 11 and 12 layer to top of atmosphere transmittances for NOAA-14 for the profiles used to train the fast model and 6 viewing angles.

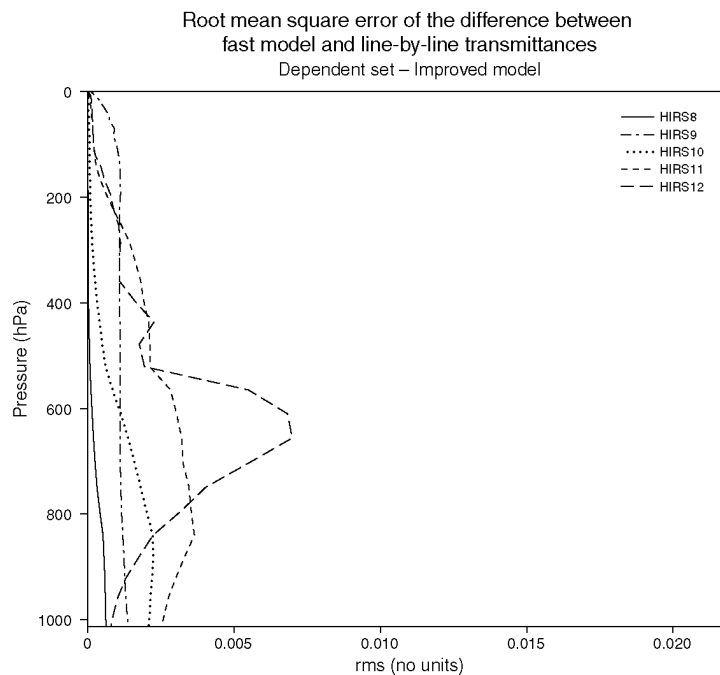


Fig 14. Root mean square of the difference between RTTOV-7 and GENLN2 HIRS channels 8, 9, 10, 11 and 12 layer to top of atmosphere transmittances for NOAA-14 for the profiles used to train the fast model and 6 viewing angles.

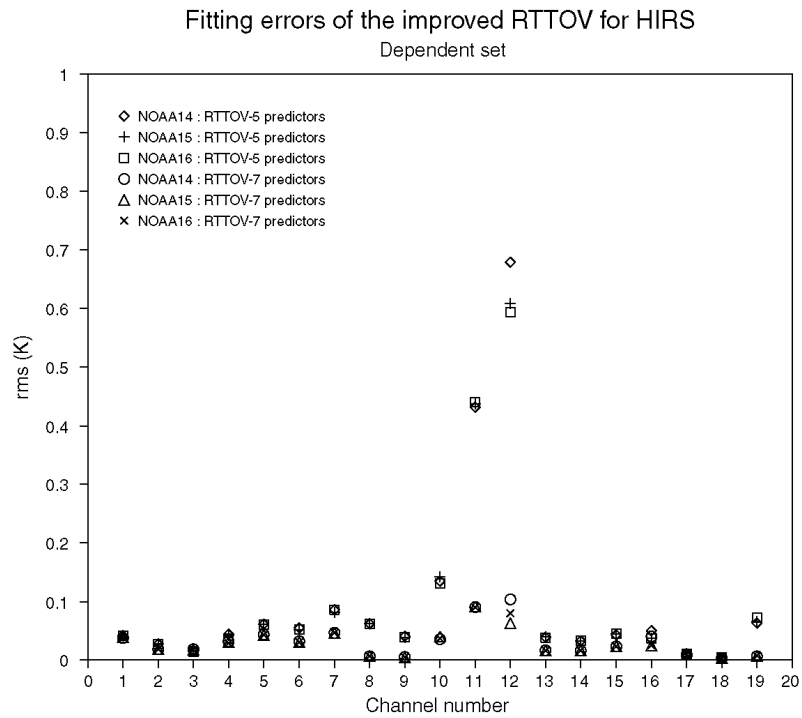


Fig 15. Root mean square of the difference between fast model and GENLN2 computed brightness temperatures for 43 diverse water vapour profiles and six viewing angles. Results are shown for RTTOV-5 and RTTOV-7. The HIRS channels of NOAA-14, NOAA-15 and NOAA-16 are plotted.

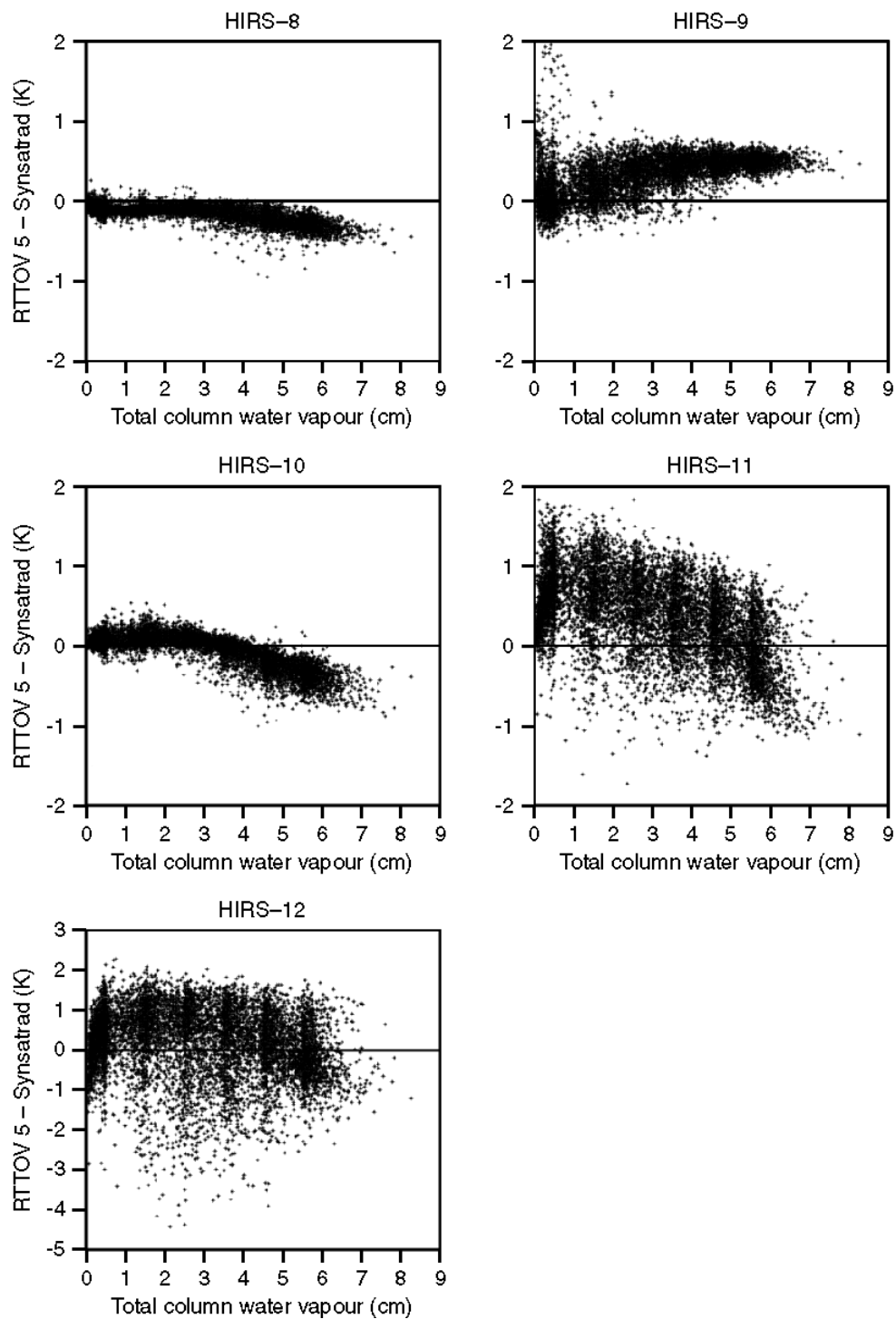


Fig 16. Difference between RTTOV-5 and Synsatrad computed brightness temperatures for 8987 independent profiles for the channels HIRS-8, HIRS-9, HIRS-10, HIRS-11 and HIRS-12 of NOAA-14.

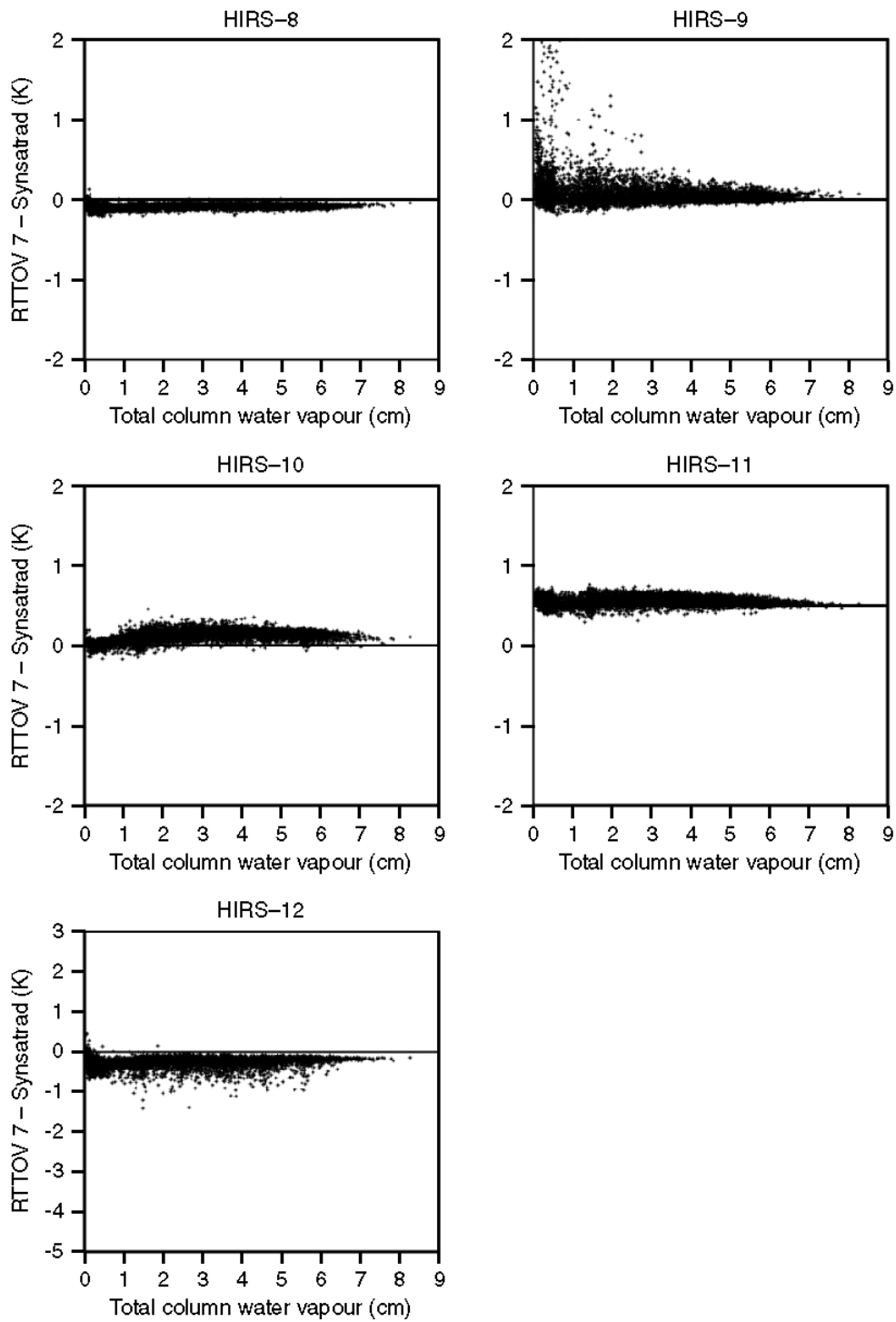


Fig 17. Difference between RTTOV-7 and Synsatrad computed brightness temperatures for 8987 independent profiles for the channels HIRS-8, HIRS-9, HIRS-10, HIRS-11 and HIRS-12 of NOAA-14.

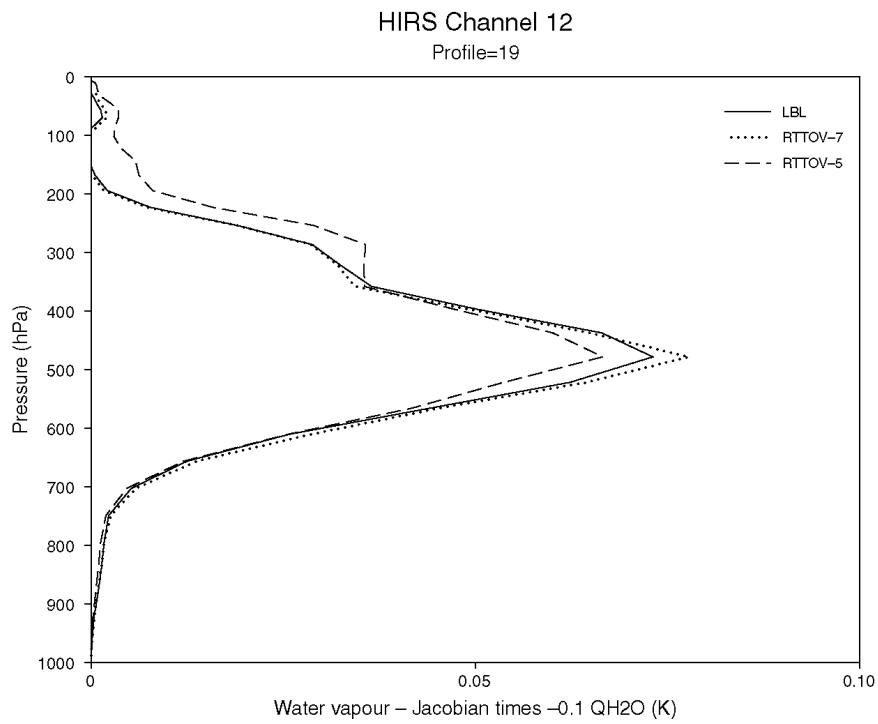


Fig 18. Water vapour Jacobian for channel HIRS-12 computed using Synstrad, RTTOV-7 and RTTOV-5.

